

A search for diffuse bands in the circumstellar envelopes of post-AGB stars[★]

R. Luna¹, N.L.J. Cox², M.A. Satorre¹, D. A. García Hernández³, O. Suárez⁴, and P. García Lario²

¹ Laboratorio de Astrofísica Experimental. Escuela Politécnica Superior de Alcoy, Universidad Politécnica de Valencia, Plaza de Ferrándiz y Carbonell, E-03801 Alcoy, Alicante, Spain

² Herschel Science Centre. Research and Scientific Support Department of ESA, European Space Astronomy Centre, P.O. Box 78, 28691, Villanueva de la Cañada, Madrid, Spain

³ W. J. McDonald Observatory. The University of Texas at Austin. 1 University Station, C1400. Austin, TX 78712-0259, USA

⁴ LUAN, Université de Nice Sophia Antipolis, Parc Valrose, 06108 Nice cedex 2, France

Received 27 March 2006; accepted 6 November 2007

ABSTRACT

In this work we present the results of a systematic search for diffuse bands (DBs, hereafter) in the circumstellar envelopes of a carefully selected sample of post-AGB stars. We concentrated on the analysis of 9 of the DBs most commonly found in the interstellar medium. The strength of these features is determined using high resolution optical spectroscopy and the results obtained are compared with literature data on field stars affected only by interstellar reddening. Based on the weak features observed in the subsample of post-AGB stars dominated by circumstellar reddening we conclude that the carrier(s) of these DBs must not be present in the circumstellar environment of these sources, or at least not under the excitation conditions in which DBs are formed. The conclusion is applicable to all the post-AGB stars studied, irrespective of the dominant chemistry or the spectral type of the star considered. A detailed radial velocity analysis of the features observed in individual sources confirms this result, as the Doppler shifts measured are found to be consistent with an interstellar origin.

Key words. Stars: AGB and post-AGB – ISM: dust, extinction – ISM: lines and bands

1. Introduction

The diffuse interstellar bands (DIBs) are absorption features, showing a broad range of widths and strengths, which appear over-imposed on the spectra of bright stars whose lines of sight probe (extra)galactic diffuse to dense interstellar clouds. Currently, more than 200 DIBs have been identified and catalogued in the spectral range from 3600 to 10200 Å (Jenniskens & Désert 1994; Cox et al. 2005), the most studied ones being those found at 4430, 5780, 5797 and 6284 Å. Since their discovery (Heger 1922), they have been associated to the interstellar medium (ISM), because their strengths show a positive relationship with the observed extinction (Merrill 1936) as well as to the neutral sodium column density (Herbig 1993). Many carriers have been proposed, however, no unambiguous identification has yet been made and it is debated whether they arise from the dust or the gas component of the ISM (see reviews by Herbig 1995 and Sarre 2006). There is increasing observational evidence that the DIB carriers constitute a set of carbonaceous gas phase molecules as evidenced from

substructures resembling rotational contours in some bands (Sarre et al. 1995, Ehrenfreund & Foing 1996). In particular, photo-UV-resistant organic molecules, such as carbon chains (Douglas 1977), PAHs (Salama et al. 1999; Allamandola et al. 1999), fullerenes (Foing & Ehrenfreund 1994; Iglesias-Groth 2007) and / or buckyonions (Iglesias-Groth 2004) are promising candidates. The local interstellar environmental conditions set the balance of local formation and destruction of the carriers as well as their level of ionization and hydrogenation. The interstellar radiation field is one of the most important factors in this (Ruiterkamp et al. 2005).

There is a possible link between the DIB carriers and the carriers of the unidentified (aromatic) infrared bands (UIBs), the so-called PAH-DIB hypothesis (Crawford et al. 1985; Leger & D'Hendecourt 1985; Van der Zwet & Allamandola 1985).

Thus, although PAHs are thought to reside and to be processed (ionisation, dehydrogenation, destruction) in the diffuse ISM, this does not exclude the scenario that these molecules (or their parent species) are produced elsewhere. Since circumstellar shells are sources of replenishment of the ISM, it has been argued that DIBs (and/or parent structures) may have a circumstellar origin, either in dense stellar winds or circum-

Send offprint requests to: R. Luna, e-mail: ralunam@fis.upv.es

[★] Based on observations collected at the European Southern Observatory (Chile) and at the Spanish Observatorio del Roque de los Muchachos of the Instituto de Astrofísica de Canarias.

stellar shells, thus somehow contravening the name they were initially given. The suspected connection between DIB carriers and some carbon-rich compounds can be investigated attending to the usually known chemistry and physical properties of these circumstellar shells.

Observationally, the detection of diffuse bands (DBs, hereafter) around evolved stars is hampered by the fact that most of them are mass-losing stars, usually strongly variable, and surrounded by very cool extended atmospheres where molecules are the dominant source of opacity. These stars are very difficult to model and DBs are hardly detected (in absorption) against the forest of features attributed to molecular transitions which appear over-imposed on the stellar continuum. This has hampered the systematic search for DBs in evolved stars in the past. Furthermore, if detected, it is difficult to determine whether the DBs are originating from the interstellar or the circumstellar environment, or even both.

In face of these difficulties Snow & Wallerstein (1972) and Snow (1973) searched for circumstellar diffuse bands (at 4430, 5780, 5797 and 6614 Å) in 26 stars with suspected circumstellar dust shells / envelopes but found no evidence for their presence. Several other authors have since searched for and commented on the presence of diffuse bands and their interstellar or circumstellar nature, in spectra observed towards planetary nebulae (NGC 6210, NGC 7027, IC 351 and AFGL 2688 by Prichet & Grillmair 1984; IRAS 21282+5050 by Cohen & Jones 1987; NGC 7027 and IRAS 21282+5050 by Le Bertre & Lequeux 1992), a post-AGB star (HR 4049; Waters et al. 1989), and a carbon star (IRAS 07270-1921 or CGCS 1732; Le Bertre 1990). Le Bertre & Lequeux (1993) studied a new sample consisting of carbon-, oxygen- or nitrogen-rich mass-losing sources, such as (pre)planetary nebulae (BD+30 3639, CPD-56 8032, Hen 104), a carbon rich RV Tauri star (AC Her), wolf-rayet stars (WR137, WR140) and post-AGB stars (HR 4049, HD213985), revisiting several sources studied in the past (*e.g.* CS 776, NCG 7027, HR 4049, IRAS 21282+5050). These authors did not find any evidence for circumstellar DBs and refuted previous claims and thus concluded that DBs are depleted in circumstellar environments. Notably, these authors did not detect any bands in the spectra of sources showing strong PAH emission (UIB) at mid-infrared wavelengths. This suggested that carrier molecules, if present, in circumstellar envelopes are in a different state of ionization / hydrogenation than in the ISM. Strong DBs were detected toward carbon-rich sources that do not show PAH emission, as well as toward most of their oxygen-rich and nitrogen-rich sources in the sample, although in all cases the observed DBs could be attributed to the interstellar material in the lines of sight. For unexplained reasons enhanced DBs were detected toward WN stars and LBVs. Exceptionally, narrow emission features possibly related to DIBs as well have been observed toward the Red Rectangle (Scarrott et al. 1992), although their identification and nature remains controversial.

A largely unexplored alternative exists. This concerns the so-called post-AGB stars that are in a short-lived transition phase between the Asymptotic Giant Branch (AGB) and the Planetary Nebula (PN) stage, evolving very rapidly in the H-R diagram while they are still surrounded by the remnant of

the AGB circumstellar shell. Post-AGB stars show all possible spectral types from M to B in what probably represents an evolutionary sequence of increasing effective temperature in their way to become PNe (García-Lario et al. 1997b). This means that in these stars we should easily be able to detect DBs formed in the remnant AGB shell over-imposed on the intermediate or early-type spectrum of the central star without the confusion originating from the presence of molecular bands in AGB stars. Interestingly, while many of these DBs are common to those observed in the ISM, the relative ratios are sometimes found to be very different (García-Lario et al. 1999). These circumstellar DBs could form and survive for some time under conditions which might be substantially different to those found in the ISM in terms of density, UV radiation field, etc. and could hold the key to understand and solve this long-standing problem. Another advantage is the fact that the chemical composition of the gas and dust in these shells can easily be determined from observations in the optical, infrared, mm / sub-mm or radio wavelengths. In addition, post-AGB stars are located in many cases at relative high galactic latitudes, and are as such affected only by little interstellar reddening. This facilitates the attribution of a circumstellar origin to the features observed.

The potential formation of DBs around post-AGB stars has, however, been explored so far only occasionally for a limited number of sources. Nevertheless, the presence of strong DBs has been reported in the optical spectra of a few post-AGB stars (Le Bertre & Lequeux 1993; García-Lario et al. 1999; Zacs et al. 1999a, 2001; Klochkova et al. 1999, 2000; Kendall et al. 2002) and some carbon rich (barium) stars (Zacs et al. 2003). In several cases tentative claims have been put forward of DBs detected at radial velocities coinciding with the photospheric absorption lines or shell/envelope expansion velocity (IRAS 04296+3429 by Klochkova et al. 1999; and HD 179821 by Zacs et al. 1999a). All other studies listed above gave non-conclusive results.

Another method recently employed utilised nearby background stars to probe the circumstellar environments of the carbon star IRC+10216 (Kendall et al. 2002) and the Helix PN (Mauron & Kendall 2004). Again, no circumstellar DBs were detected, confirming the lack of DIB carriers in these environments.

In this work we present the first systematic survey to detect the presence of circumstellar DBs (DCBs) in a carefully selected sample of galactic post-AGB stars¹. The goal is to perform a detailed analysis of the differential properties observed in the DBs associated to post-AGB stars in comparison with the standard DBs observed towards reddened, early-type field stars (where these bands are expected to be essentially of interstellar origin).

To perform this task we have studied the intensity of 9 of the strongest absorption features identified as DBs in the spectral range 4000–10000 Å using high resolution optical spectroscopy. The comparison of the properties observed in carbon-rich and oxygen-rich post-AGB stars is used to test the carbon-

¹ The sample also includes three very young planetary nebulae, which are here also considered post-AGB stars in a broad sense.

Table 1. Observation log.

Name	Other Names	Observing Date	Observatory	Telescope	Instrument	Spectral range (Å)	Resolution
IRAS 01005+7910		12.09.03	La Palma	TNG (3.58 m)	SARG	4960–10110	50000
IRAS Z02229+6208		12.09.03	La Palma	TNG (3.58 m)	SARG	4960–10110	50000
IRAS 04296+3429		22.08.94	La Palma	WHT (4.2 m)	UES	5570–10200	55000
IRAS 05113+1347		23.02.94	La Palma	WHT (4.2 m)	UES	4480–10200	55000
IRAS 05251-1244	IC 418	12.09.03	La Palma	TNG (3.58 m)	SARG	4960–10110	50000
IRAS 05341+0852		30.09.98	ESO-La Silla	NTT (3.58 m)	EMMI	5570–10040	65000
IRAS 06530-0213		12.01.01	ESO-Paranal	VLT-U2 (8 m)	UVES	4790–6810	100000
IRAS 07134+1005	HD 56126	20.12.93	La Palma	WHT (4.2 m)	UES	3980–10400	55000
IRAS 08005-2356		02.03.94	La Palma	WHT (4.2 m)	UES	3690–11050	55000
IRAS 08143-4406		16.01.01	ESO-Paranal	VLT-U2 (8 m)	UVES	3750–10520	100000
IRAS 08544-4431		26.01.99	ESO-La Silla	ESO-1.52	FEROS	3700–8860	50000
IRAS 12175-5338	SAO 239853	24.03.00	ESO-La Silla	ESO-1.52	FEROS	3730–8850	50000
IRAS 16594-4656		20.05.00	ESO-Paranal	VLT-U2 (8 m)	UVES	3750–10520	100000
IRAS 17086-2403		14.07.01	La Palma	WHT (4.2 m)	UES	4300–9000	50000
IRAS 17097-3210	HD 155448	07.07.97	ESO-La Silla	NTT (3.58 m)	EMMI	5800–10430	60000
IRAS 17150-3224	RAFGL 6815	10.06.00	ESO-Paranal	VLT-U2 (8 m)	UVES	3750–10520	100000
IRAS 17245-3951		21.05.00	ESO-Paranal	VLT-U2 (8 m)	UVES	3750–10520	100000
IRAS 17395-0841		13.07.01	La Palma	WHT (4.2 m)	UES	4300–9000	55000
IRAS 17423-1755	Hen 3-1475	13.07.01	La Palma	WHT (4.2 m)	UES	4300–9000	55000
IRAS 17436+5003	HD 161796	01.09.94	La Palma	WHT (4.2 m)	UES	3650–10200	55000
IRAS 18025-3906		30.09.98	ESO-La Silla	NTT (3.58 m)	EMMI	3980–10430	65000
IRAS 18062+2410	HD 341617	13.07.01	La Palma	WHT (4.2 m)	UES	4300–9000	50000
	HD 172324	08.08.95	ESO-La Silla	NTT (3.58 m)	EMMI	3650–10240	55000
IRAS 19114+0002	HD 179821	07.07.97	ESO-La Silla	NTT (3.58 m)	EMMI	5800–10430	60000
IRAS 19200+3457	LS II +34 1	11.09.03	La Palma	TNG (3.58 m)	SARG	4960–10110	50000
IRAS 19386+0155		30.09.98	ESO-La Silla	NTT (3.58 m)	EMMI	5980–8320	65000
IRAS 19500-1709	HD 187885	07.08.95	ESO-La Silla	NTT (3.58 m)	EMMI	3650–10040	55000
IRAS 20000+3239		23.08.94	La Palma	WHT (4.2 m)	UES	4440–10040	50000
IRAS 20462+3416	LS II +34 26	17.08.96	La Palma	WHT (4.2 m)	UES	5300–9380	55000
IRAS 22023+5249	LS III +52 24	14.07.01	La Palma	WHT (4.2 m)	UES	4300–9000	55000
IRAS 22223+4327	BD+42 4388	24.08.94	La Palma	WHT (4.2 m)	UES	4440–10040	50000
IRAS 22272+5435	HD 235858	23.08.94	La Palma	WHT (4.2 m)	UES	4440–10220	55000
IRAS 23304+6147		23.08.94	La Palma	WHT (4.2 m)	UES	4440–10040	55000

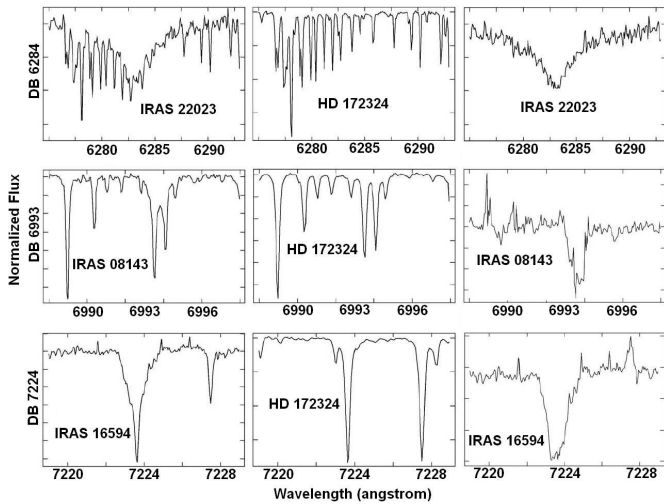


Fig. 1. Removal of telluric lines at 6284, 6993 and 7224 Å. A few examples are shown before (left) and after correction (right). In the middle panel we show the stellar spectrum of HD 172324 (B9Ib), one of the sample stars, which was used as telluric divisor (see text).

rich nature of the DB carrier(s) and determine which of the DBs detected are most probably of circumstellar origin (if any).

In Section 2 we describe the observations made and the data reduction process. The strategy followed in our analysis is presented in Section 3. The main results are discussed in Section 4 as a function of various observational parameters. Finally, the conclusions are presented in Section 5.

2. Observations and Data Reduction

The high-resolution Echelle spectroscopic data analysed in this paper were taken using a wide variety of instruments and telescopes over the period 1993–2003. Originally, these observations were carried out for chemical abundance analysis purposes and they correspond to observations performed using the Utrecht Echelle Spectrograph (UES) at the William Herschel Telescope (WHT 4.2m) and the High Resolution Spectrograph (SARG) at the Telescopio Nazionale Galileo (TNG 3.58m), both in the Spanish Observatorio del Roque de los Muchachos (La Palma, Spain); the UV-Visual Echelle Spectrograph (UVES) installed at the Very Large Telescope-U2 (VLT 8m) in Paranal Observatory (Chile); and the ESO Multi-Mode Instrument (EMMI) at the New Technology Telescope (NTT 3.5m) and the Fiber-fed Extended Range

Table 2. Main characteristics of the post-AGB stars selected for the analysis

IRAS Name	$E(B - V)$	Ref.	Chemistry	Ref.	Sp.Type	Ref.	GLON.	GLAT.
01005+7910	0.2 ± 0.1	(25)	C	(25)	B2	(25)	123.57	+16.59
02229+6208	1.67 ± 0.09	(17)	C	(37)	G9Ia	(37)	133.73	+1.50
04296+3429	1.3 ± 0.1	(7, 15, 36)	C	(27)	G0Ia	(3)	166.24	-9.05
05113+1347	1.1 ± 0.2	(26, 36, 40)	C	(26)	G5I	(40)	188.86	-14.29
05251-1244	0.23 ± 0.09	(35)	C	(42)	PN/07f	(14)	215.21	-24.28
05341+0852	1.65 ± 0.09	(7, 17, 40)	C	(26)	F5I	(15)	196.19	-12.14
06530-0213	1.7 ± 0.2	(36, 40)	C	(18)	F5I	(18)	215.44	-0.13
07134+1005	0.4 ± 0.1	(15, 40)	C	(26)	F7 Ie	(40)	206.75	+9.99
08005-2356	0.7 ± 0.3	(15, 40)	O	(5)	F5I	(3)	242.36	+3.58
08143-4406	0.8 ± 0.1	(36, 40)	C	(39)	F8I	(36)	260.83	-5.07
08544-4431	1.45 ± 0.09	(29)	O	(29)	F3	(29)	265.50	+0.39
12175-5338	0.25 ± 0.09	(19, 38)	C	(46)	A9Iab	(32)	298.30	+8.67
16594-4656	2.2 ± 0.3	(20, 40, 44)	C	(9)	B7	(44)	340.39	-3.29
17086-2403	0.86 ± 0.09	(40)	C?	(10)	PN+G5?	(34)	359.84	+8.99
17097-3210	0.06 ± 0.05	(30)	C	(45)	B9	(30)	353.36	+4.03
17150-3224	0.68 ± 0.09	(23)	O	(23)	G2I	(23)	353.84	+2.98
17245-3951	1.0 ± 0.1	(40)	O	(20)	F6I	(40)	348.81	-2.84
17395-0841	1.1 ± 0.2	(11, 40)	O?	(10)	PN+G	(11)	17.02	+11.10
17423-1755	1.13 ± 0.09	(11, 40)	O	(41)	Be	(11)	9.36	+5.78
17436+5003	0.24 ± 0.09	(19)	O	(4)	F3 Ib	(48)	77.13	+30.87
18025-3906	1.15 ± 0.09	(22, 40)	O	(24)	G1I	(40)	353.27	-8.72
18062+2410	0.6 ± 0.2	(33, 40)	O	(33)	B1 I	(33)	50.67	+19.79
HD 172324	0.03 ± 0.02	(6)	O	(1)	B9Ib	(1)	66.18	+18.58
19114+0002	0.60 ± 0.05	(19, 40)	O	(4)	G5 Ia	(3)	35.62	-4.96
19200+3457	0.3 ± 0.1	(11)	O?	(11)	B	(11)	67.57	+9.51
19386+0155	1.05 ± 0.09	(2)	O	(28)	F5I	(31)	40.51	-10.09
19500-1709	0.37 ± 0.09	(19)	C	(47)	F2-6 Ia	(3)	23.98	-21.04
20000+3239	1.6 ± 0.1	(15, 26)	C	(21)	G8Ia	(21)	69.68	+1.16
20462+3416	0.38 ± 0.09	(8, 43)	O	(8)	B1.5	(8)	76.60	-5.75
22023+5249	0.52 ± 0.09	(12)	O	(13)	B	(12)	99.30	-1.96
22223+4327	0.2 ± 0.1	(15, 26)	C	(26)	G0 Ia	(15)	96.75	-11.56
22272+5435	0.9 ± 0.2	(15)	C	(16)	G5 Ia	(15)	103.35	-2.52
23304+6147	1.4 ± 0.2	(15, 36)	C	(15)	G2 Ia	(15)	113.86	+0.59

- | | | | |
|-----------------------------------|-----------------------------------|-----------------------------------|--------------------------------------|
| (1) Arellano et al. (2001) | (13) Gauba & Parthasarathy (2004) | (25) Klochkova et al. (2002) | (37) Reddy et al. (1999) |
| (2) Arkhipova et al. (2000) | (14) Heap & Augensen (1987) | (26) Kwok et al. (1995) | (38) Reed & Vance (1996) |
| (3) Bakker et al. (1997) | (15) Hrivnak (1995) | (27) Kwok et al. (1999) | (39) Reyniers et al. (2004) |
| (4) Bujarrabal et al. (1992) | (16) Hrivnak & Kwok (1991) | (28) Lewis (2000) | (40) Suárez et al. (2006) |
| (5) Desmurs et al. (2002) | (17) Hrivnak & Kwok (1999) | (29) Maas et al. (2003) | (41) te Lintel Hekkert et al. (1991) |
| (6) Fernie (1983) | (18) Hrivnak & Reddy (2003) | (30) Malfait et al. (1998) | (42) Torres-Peimbert et al. (1980) |
| (7) Fujii et al. (2002) | (19) Hrivnak et al. (1989) | (31) Meixner et al. (1999) | (43) Turner & Drilling (1984) |
| (8) García-Lario et al. (1997a) | (20) Hrivnak et al. (1999) | (32) Oudmaijer et al. (1992) | (44) van de Steene & van Hoof (2003) |
| (9) García-Lario et al. (1999) | (21) Hrivnak et al. (2000) | (33) Parthasarathy et al. (2000a) | (45) van der Veen et al. (1989) |
| (10) García-Lario (priv.comm.) | (22) Hu et al. (1993a) | (34) Parthasarathy et al. (2000b) | (46) van Winckel (1997) |
| (11) Gauba et al. (2003) | (23) Hu et al. (1993b) | (35) Pottasch et al. (2004) | (47) van Winckel & Reyniers (2000) |
| (12) Gauba & Parthasarathy (2003) | (24) Hu et al. (1994) | (36) Reddy & Parthasarathy (1996) | (48) Volk & Kwok (1989) |

Optical Spectrograph (FEROS) at the ESO 1.52m telescope in La Silla Observatory (Chile).

The spectra obtained cover a wide wavelength range (usually from 4000 to 10000 Å) with a resolving power in the range 50000–100000 at 5500 Å, depending on the instrument set-up. The exposure times are variable, depending on the brightness of the source, but typically of ~ 30 min, leading to a signal-to-noise of 20–200 over the spectral range considered.

The two-dimensional spectra were reduced following the standard procedure for echelle spectroscopy using IRAF astronomical routines. The process includes: identification of bad pixels, bias determination and scattered light subtraction, flat-

field correction, order extraction and wavelength calibration. For the DBs at 6284, 6993 and 7224 Å, strongly affected by terrestrial features, the spectrum of HD 172324 (B9Ib), one of the sample stars very little affected by extinction, was used as divisor to remove the telluric absorption lines² (see Figure 1).

² Note that the initial strategy was to use the spectrum of a hot, rapidly rotating star observed on the same night for this purpose, but it was found that the latter showed faint but detectable DBs in its spectrum which did not allow us to perform this correction properly. In contrast, the 6284, 6993 and 7224 Å DBs were found to be totally absent in HD 172324.

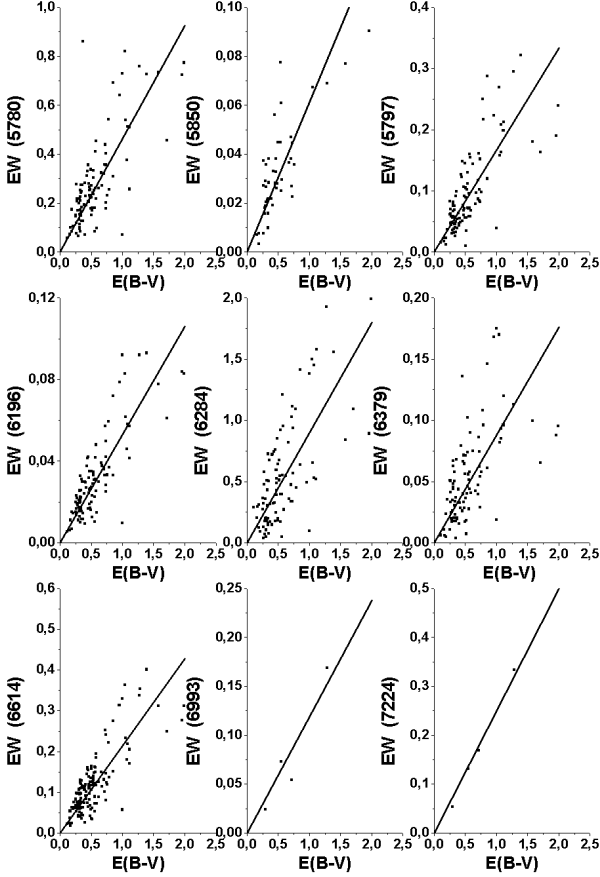


Fig. 2. Equivalent width measurements taken from the literature for field stars, plotted as a function of $E(B - V)$. Table 3 gives slopes $EW/E(B - V)$ and correlations r for the linear fits.

3. Selection of the sample

In order to make a systematic study of the presence of DCBs in post-AGB stars, we carefully selected a sample of 33 sources from the literature trying to cover as much as possible a wide variety of observational properties such as the chemistry of the circumstellar envelope (carbon-rich and oxygen-rich) or the spectral type of the central stars³. Priority was given to sources located at high galactic latitudes showing a strong colour excess $E(B - V)$ (as these sources are most likely dominated by circumstellar extinction) and to those for which a high radial velocity has been reported in the literature (since this may later facilitate the identification of spectral features of circumstellar origin).

The main objective is to understand whether systematic differences are detected which depend on one (or more) of the above observational parameters.

The list of stars selected for analysis, most of them IRAS sources belonging to the GLMP catalogue of post-AGB stars (García-Lario et al. 1997a; Suárez 2004), is displayed in Table 1, where a summary description of the observations made

³ Stars with spectral types later than G- were discarded for the analysis, as their continuum is dominated by the presence of molecular bands, which makes the identification of DBs a very difficult task.

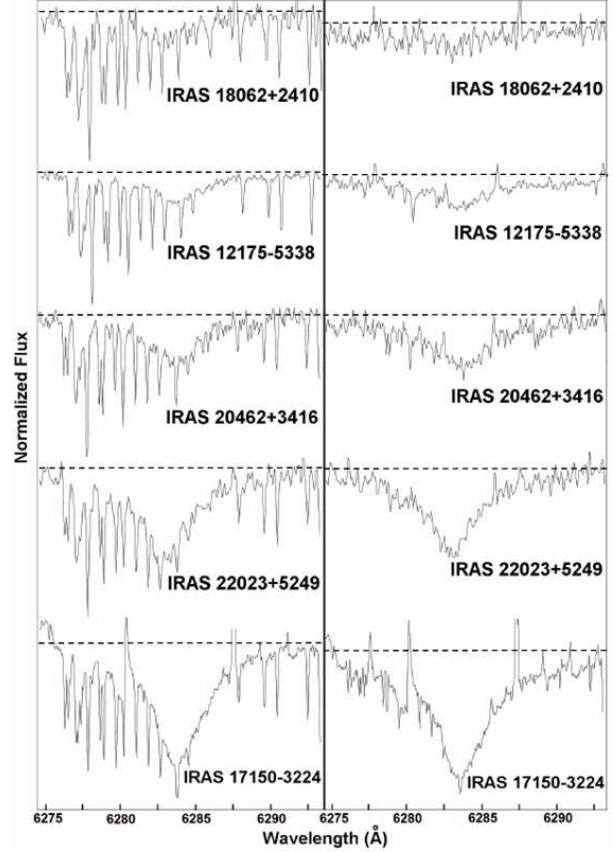


Fig. 3. Sample spectra showing the region around the DB at 6284 Å, before (left panel) and after (right panel) removal of the telluric lines using as the telluric divisor HD 172324. Dotted lines indicate the continuum level adopted in each case.

is presented. In Table 2, additional information is given on the sources included in our observing programme. This includes the colour excess $E(B - V)$, dominant chemistry (carbon-rich or oxygen-rich), spectral type and galactic coordinates (GLON, GLAT), as well as the bibliographic references from where this information was extracted.

The spectral regions corresponding to 9 different DBs which are among the strongest ones reported in the literature have been investigated in detail for each of the sources included in our sample. Table 3 lists the accurate wavelengths (λ_0) corresponding to each of these features, taken from Galazutdinov et al. (2000), as well as their central depth A_c and sensitivity to the extinction, measured as $EW/E(B - V)$, observed toward the star HD 183143 (B7I; $E(B - V) = 1.28$ mag), which is usually taken as the prototype star in the analysis of DIBs (Herbig 1995). All the DBs selected for analysis are within the optical domain, and they are referred to in the literature as the 5780, 5797, 5850, 6196, 6284, 6379, 6614, 6993 and 7224 Å features. Other well known DBs at 4430 and 6177 Å are even stronger than the selected ones, but they have been discarded for study because of the difficulty to detect their extremely broad (and relatively shallow) profiles ($FWHM > 17$ Å; $A_c < 0.1$) in our high resolution spectra.

Table 3. Main characteristics of the selected DBs (central depth A_c and normalised equivalent width $EW/E(B - V)$), as measured towards the prototype star HD 183143 (Herbig 1995) (cols. 3 and 4). The reference wavelengths are taken from Galazutdinov et al. (2000) (col. 2). The equivalent width per extinction unit (this work) derived from published data from Jenniskens & Désert (1994), Weselak et al. (2001), Thorburn et al. (2003) and Megier et al. (2005) is given for each DB in col. 5, with corresponding correlation coefficients in col. 6.

DB (Å)	λ_0 (Å)	HD 183143		this work	
		A_c	$EW/E(B - V)$ (Å/mag)	$EW/E(B - V)$ (Å/mag)	r
5780	5780.37	0.32	0.63	0.46	0.74
5797	5796.96	0.20	0.19	0.17	0.73
5850	5849.80	0.069	0.06	0.061	0.75
6196	6195.96	0.084	0.06	0.053	0.82
6284	6283.85	0.32	1.5	0.90	0.69
6379	6379.29	0.10	0.096	0.088	0.62
6614	6613.56	0.24	0.29	0.21	0.80
6993	6993.18	0.14	0.14	0.12	0.95
7224	7224.00	0.21	0.29	0.25	0.99

$$A_c = 1 - F(\lambda_0) / F(\text{continuum})$$

4. Discussion

4.1. DB strength vs. extinction in field stars

Although it is generally accepted that there is a tight correlation between the equivalent width of DBs and the value of $E(B - V)$ in field stars dominated by interstellar reddening, the available results in the literature generally cover only the stronger DBs ($\lambda\lambda$ 4430, 5780, 5797 and 6284). In addition, they are usually based on old data obtained with poor spectroscopic resolution (sometimes, even below $R = 1000$). Unfortunately, studies covering other DBs and/or based on high resolution spectroscopy are scarce. Prior to derive any conclusion on the existence (or not) of a similar correlation between DB strength and extinction in our sample of post-AGB stars it is, thus, necessary to establish this dependency for each of the 9 DBs observed toward field stars.

For this purpose, we have re-derived ourselves these correlation parameters using a large number of early-type stars taken from Weselak et al. (2001); Thorburn et al. (2003) and Megier et al. (2005), for which accurate DB strength measurements are available covering a wide range of extinction values. Weselak et al.'s sample contains 41 stars observed at $R \sim 64000$, for which equivalent width data are available corresponding to the DB centred at 6614 Å. Thorburn et al.'s sample comprises 53 stars observed with spectral resolution $R \sim 38000$, that were originally used to study the DBs centred at 5780, 5797, 6196, 6284, 6379 and 6614 Å. Finally, Megier et al.'s sample comprises 49 stars observed with spectral resolution $R \sim 64000$, that were originally used to study the DBs centred at 5780, 5797, 5850, 6196, 6284, 6379 and 6614 Å. Four additional stars taken from Jenniskens & Désert (1994), observed at $R \sim 20000$, were also used to derive the correlation parameters associated to the

DBs centred at 6993 and 7224 Å, for which measurements are much more scarce in the literature. The sources included in these four samples are expected to follow a behaviour representative of field stars affected only by interstellar extinction. Figure 2 shows all the equivalent width measurements used in our analysis, plotted as a function of the interstellar extinction, measured as $E(B - V)$.

For each DB under analysis we have applied a linear fit to the data available. We have also imposed the condition $EW = 0$ for $E(B - V) = 0$, i.e.: $EW = a \cdot E(B - V)$, where a is a constant that represents the equivalent width per extinction unity. In practice this is equivalent to assume that there is a direct link between the DB carrier(s) and the material which is responsible for the extinction observed in the ISM. The fits obtained represent the DB strength expected as a function of the colour excess for any given source in which interstellar reddening is the dominant contributor to the overall extinction. These are represented by solid lines in Figure 2. The slopes ($EW/E(B - V)$) and correlation coefficients r of the linear fits are given in Table 3.

As we can see, a reasonable correlation between equivalent width and $E(B - V)$ is always found, although the dispersion is in some cases considerable. The new results obtained are in agreement as well with those derived for the prototype star HD 183143 by (Herbig 1995) although the 5780 and 6284 DBs are significantly stronger toward the latter, probably due to local environmental conditions. These results provide confidence to proceed with the study of the post-AGB stars in our sample, based on the assumption that the above values can be taken as references for the subsequent analysis.

4.2. DB strength vs. extinction in post-AGB stars

In Table 5 (Online only) we show the equivalent width of each of the 9 DBs considered in our analysis for every post-AGB star in the sample, as determined from the available high resolution spectra. Note that three of these bands are strongly affected by telluric contamination, namely those centred at 6284, 6993 and 7224 Å. For these features, a careful removal of the telluric component was performed prior to the determination of their EW (see Figures 1 and 3; Sect. 2). For the other DBs, the measurements were performed directly on the normalised spectra. We note here that in none of the spectra we found evidence for DB features in emission.

The resulting values are plotted in Figure 4 as a function of the colour excess $E(B - V)$. The values of $E(B - V)$ which were used to produce this figure are directly taken from the literature (see Table 2) or estimated from the available information on spectral type and photometry by comparing the observed B and V magnitudes with the intrinsic $B - V$ colours expected for stars of the same spectral type and luminosity class I⁴.

⁴ A luminosity class I is adopted because this is the class corresponding to low-gravity stars, but note that post-AGB stars only look like super-giants, but they are not genuine population I massive super-giant stars (Fitzgerald 1970). Values quoted by different authors are generally in good agreement, and the discrepancies found, when relevant, are reflected in the associated errors provided in Table 2.

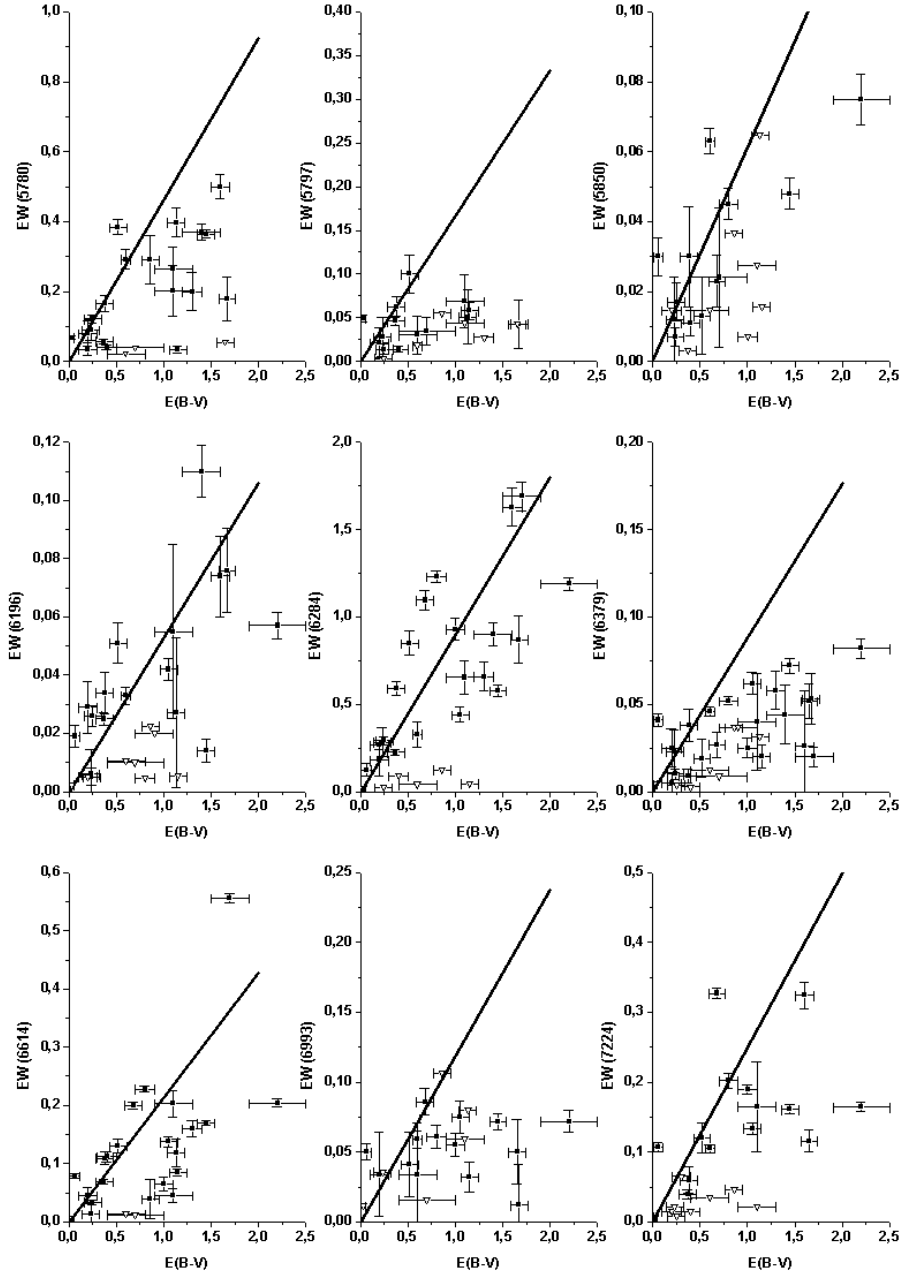


Fig. 4. Equivalent width (in Å) of the 9 DBs selected for analysis as a function of $E(B - V)$ for the post-AGB stars in the sample. Solid lines correspond to the fits derived in this paper for field stars dominated by interstellar extinction (see also Sect. 4.1). The inverted triangles represent upper limits.

Figure 4 shows the overall results obtained for the 9 DBs studied. In general we find that the equivalent width of the observed features seems to be still correlated with the value of $E(B - V)$. However, in contrast to the results obtained for the field stars (shown in Figure 2), this correlation is now very weak in some cases and we identify a much larger number of outliers.

Usually, for a given extinction $E(B - V)$, the measured equivalent widths in post-AGB stars are well below the expected values. Only a subset of sources follow exactly the same behaviour observed in field stars. We interpret this result as the

consequence of the absence (or at least the under-abundance) of the DB carriers in the circumstellar envelopes of most of these post-AGB stars, but further analysis is needed to confirm that there is no other alternative explanation.

4.3. Interstellar vs. circumstellar extinction

In order to determine whether our preliminary hypothesis is consistent with the measurements here presented, it is necessary to take into account that in general, the overall extinction observed towards a given source in the sky is the result of the

Table 4. Line-of-sight properties for the observed post-AGB stars. DCS = dominated by circumstellar reddening; HV = high radial velocity; CS1 designated DCS based on lat/long vs reddening, excluding those that are discarded based on interstellar (IS) reddening estimate. CS2 indicates DCS found by estimating the upper limit to the IS reddening. Principal extinction estimates are given with rescaling of disk / spiral component (col. 7). No-rescaling estimates are given (col. 8) in those cases for which the extinction estimate is significantly higher than with use of rescaling. The angular scale of COBE data is $0.35^\circ \times 0.35^\circ$ and this dust extinction model therefore only gives mean extinction estimates. Erroneous rescaling factors can arise for directions toward strong extra-galactic sources such as M31, M33, SMC and LMC as well as toward peculiar galactic regions such as Orion and the Rho Ophiuchus complex. Also, lines of sight corresponding to arm tangents may have large systematic errors. Distance estimates (references in col. 4) and corresponding model extinctions (converted to $E(B - V)$) are given when available in Cols. 3 & 5). The maximum model reddening (with and without re-scaling) and the corresponding distance in the target direction are given in cols. 7, 8 and 6, respectively. Col. 9 gives the resulting lower limit for the circumstellar reddening. The final column (10) indicates when the target is dominated by circumstellar reddening (CS1 or CS2) and/or is a high velocity target (HV).

NAME	$E(B - V)$ observed	d kpc	Ref.	$E(B - V)$ IS	d_{\max} kpc	$E(B - V)$ IS scaling	$E(B - V)$ IS no scaling	$E(B - V)$ -CS min	DCS / HV
01005+7910	0.2 ± 0.1	3		0.11	1.7	0.11			
02229+6208	1.67 ± 0.09	> 2.2		0.60	5	0.99		0.68	CS2
04296+3429	1.3 ± 0.1	3.5		0.23	3.3	0.23		1.07	CS1
		5.4, 5	2, 9	0.23					
05113+1347	1.1 ± 0.2	5	9	0.14	2.1	0.14		0.96	CS1
05251-1244	0.23 ± 0.09				1	0.18			
05341+0852	1.65 ± 0.09	10	9	0.16	2.4	0.16		1.49	CS1
06530-0213	1.7 ± 0.2	3	9	0.36	5	0.41		1.29	CS2
07134+1005	0.4 ± 0.1				2.8	0.024	0.14	0.38 / 0.26	HV / CS2
08005-2356	0.7 ± 0.3				4	0.18	0.27	0.52 / 0.43	CS2
08143-4406	0.8 ± 0.1	4	9	0.55	5.8	0.66			
08544-4431	1.45 ± 0.09				6	0.99		0.46	CS2?
12175-5338	0.25 ± 0.09				3	0.24			
16594-4656	2.2 ± 0.3	2.6	10,11		7	2.1			CS (*)
17086-2403	0.86 ± 0.09	6	9	0.56	2	0.56		0.3	HV (CS2?)
17097-3210	0.06 ± 0.05	(0.2)		(0.08)	5	0.95			
17150-3224	0.68 ± 0.09	< 18 (2)	9	(0.9)	5	1.8			
17245-3951	1.0 ± 0.1				5	1.0	1.5		HV
17395-0841	1.1 ± 0.2				2	0.87		0.23	HV
17423-1755	1.13 ± 0.09	3.2 – 3.7		0.6	4	0.60		0.53	CS1 / HV
17436+5003	0.24 ± 0.09	1.2		0.03	0.9	0.026	0.064	0.18	CS1
18025-3906	1.15 ± 0.09				2	0.23	0.34	0.92 / 0.81	CS1 / HV
18062+2410	0.6 ± 0.2	4.5 – 5.3		0.14	1.4	0.14		0.46	CS1 / HV
HD 172324	0.03 ± 0.02				1.5	0.056	0.11		
19114+0002	0.60 ± 0.05	1.5	4	0.32	5	0.54	0.62		HV
19200+3457	0.3 ± 0.1				2.9	0.15	0.22		
19386+0155	1.05 ± 0.09				2.9	0.35		0.80	CS1
19500-1709	0.37 ± 0.09	> 4	12		1.0	0.20			
20000+3239	1.6 ± 0.1	(5,8)		(1.0,1.7)	>10	>1.7		?	
20462+3416	0.38 ± 0.09				4	0.25	0.38		HV
22023+5249	0.52 ± 0.09	3.3 – 3.9		0.47,0.50	5	0.52	0.55		HV
22223+4327	0.2 ± 0.1				2.6	0.21			
22272+5435	0.9 ± 0.2	1.6,2.7	8	0.26,0.39	4.5	0.47		0.43	CS2
23304+6147	1.4 ± 0.2	4.7, 5	5, 9	0.64	4.5	0.64		0.76	CS2

[1] Reddy et al. (1999); [2] Klochkova et al. (1999); [3] García-Lario et al. (1999); [4] Zacs et al. (1999a,b); [5] Klochkova et al. (2000); [6] Bakker et al. (1997); [7] Hrivnak & Kwok 1991; [8] Woodsworth et al. (1990); [9] Reddy & Parthasarathy (1996); [10] Hrivnak et al. (2000); [11] van de Steene & van Hoof (2003); [12] Clube & Gledhill (2004), $A(V)=1.2$. (*) IRAS 16594-4656 is a well known bi-polar PPN which is thought to have a high internal extinction (see also Sect. 4.3).

combined effect of the contribution coming from the ISM and of the internal extinction produced in the circumstellar shell. Making this distinction is generally not important in field stars, since for them the latter contribution is negligible. However, for the evolved stars in our sample the situation is completely

different as, in many cases, the observed reddening is almost exclusively of circumstellar origin.

Disentangling interstellar versus circumstellar extinction for a given source is a very difficult task, if we need to rely only on the available observations. The only option we have is to use a statistical approach to estimate whether the observed

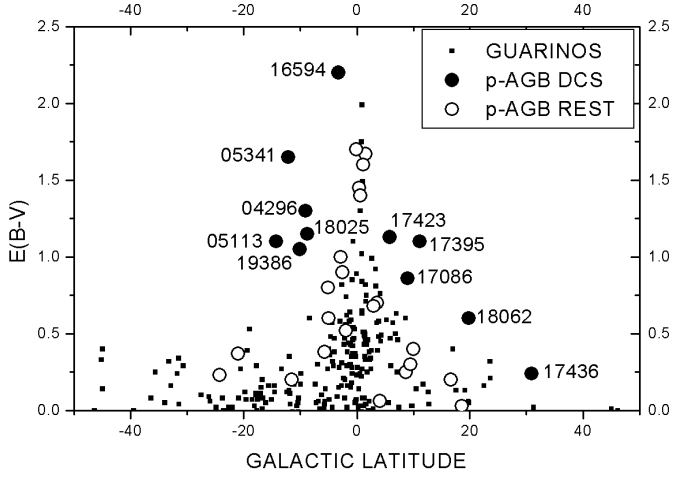


Fig. 5. $E(B - V)$ versus Galactic latitude distribution of the post-AGB stars in the sample (circles) and for reference stars taken from Guarinos (1988a,b, 1997) (small squares). Post-AGB stars dominated by circumstellar extinction (DCS-type) are indicated by filled circles and they are labeled with their IRAS name.

extinction corresponds preferentially to one or another component.

For this we have represented in Figure 5 the $E(B - V)$ versus galactic latitude distribution of the post-AGB stars in our sample and compared this distribution with that shown by field stars taken from the catalogue of Guarinos (Guarinos 1988a,b, 1997). This catalogue, also used for the study of DB strengths, contains observations of 270 early-type field stars homogeneously distributed along the Galactic Plane (but excluding the Galactic Bulge), located at a variety of galactic latitudes and for which the value of $E(B - V)$ has previously been determined.

Figure 5 shows clearly that a subsample of post-AGB stars are clear outliers in this plot. This indicates that the reddening excess in these stars must be circumstellar in origin. Other sources, however, show a relatively small reddening fully compatible with the values observed in field stars located at the same galactic latitude.

Based on this analysis, we have divided our sample of post-AGB stars in two groups according to whether the overall extinction observed is more likely to be dominated by the circumstellar contribution (DCS-type stars; filled circles in Figure 5; CS1 in Table 4) or just consistent with the interstellar extinction expected according to its Galactic Latitude (rest of stars; indicated by open circles in Figure 5).

Note that the above classification is very rough and that it just considers a star as belonging to the DCS group if it shows a relative large reddening excess with respect to the nominal value expected from its galactic location. Stars in which there is only a moderate (although possibly significant) contribution from the circumstellar shell to the observed extinction may have escaped detection. This means that the group of stars not classified in the DCS group may still contain sources in which the circumstellar contribution to the observed reddening is not

negligible, and vice versa, those classified DCS may still contain a significant interstellar dust contribution.

In order to estimate an upper limit to the contribution of the interstellar reddening to the total reddening we use the Galactic 3D-extinction model map by Drimmel et al. (2003) that gives the *mean* visual extinction as a function of sky (galactic) coordinates and distance. The extinction has a projected resolution of $0.35^\circ \times 0.35^\circ$ (this is set by the COBE map which is used to re-scale the extinction in order for the model to reproduce correct far-infrared flux). It is evident that any small scale structure (including the circumstellar contribution of the target star) is washed out in these estimates, which nevertheless give us information on the *global* spatial distribution of dust in specific directions. We take distance estimates from literature where possible (column 3 in Table 4) and/or extract the maximum extinction (column 7) and the corresponding distance (column 6) for a particular line-of-sight. For high latitudes the extinction versus distance curve flattens rapidly, within a few kpc. These (upper limit) estimates for the interstellar visual extinction, converted to reddening by dividing by the canonical value for $R_V = 3.1$, can then be subtracted from the total observed reddening and thus yield (lower limit) estimates for the circumstellar reddening (column 9). Caution is needed when applying these results to derive extinction values for individual sightlines. Notwithstanding, we can now review and improve our (statistical) classification based on reddening versus latitude.

We consider all targets that are estimated to have a (lower limit) circumstellar reddening contribution higher than 50% of the total observed reddening to be of DCS-type (CS2 in Table 4). From the 11 DCS-type targets previously selected, on basis of their latitude reddening excess, we find that 9 satisfy this criterion. For the other 2 targets we can attribute a high fraction of the total observed reddening to interstellar dust.

Among the 22 IS (interstellar) reddening dominated targets selected above via their latitude we find 7 targets with a non-negligible circumstellar reddening $E(B - V)_{CS} \geq 0.4$ mag (Table 4; indicated CS2).

IRAS 02229+6208 and IRAS 08544-4431 are special cases because these lines-of-sight show both a strong interstellar and circumstellar dust contribution.

4.4. DB strength in DCS-type post-AGB stars

Following the above criteria, we find that for 17 (out of 33) stars in the sample a significant fraction of the observed reddening is due to the presence of circumstellar dust (i.e. DCS-type), while for the remaining targets the colour excesses are expected to be predominantly due to interstellar dust.

A comparison of the DB strengths measured in stars belonging to each of the two groups considered above with those found in reference field stars is presented in Figure 6, where we can see that there is a general trend for the stars with a dominant circumstellar extinction contribution (DCS-type) to show much weaker DB strengths compared to the rest of post-AGB stars in the sample. In the most extreme cases, there are stars in this group affected by a large overall extinction in which surpris-

ingly some DBs are completely absent, and only upper limits to their equivalent width can be reported. In contrast, we find a significant number of sources among the rest of post-AGB stars in the sample showing DB strengths fully in agreement with those observed in field stars.

For many cases DBs are observed towards the DCS-type stars (Figs. 7 to 15; left panels). In order to assess the circumstellar contribution the observed EW can be corrected by subtracting the expected DIB EW found by applying the estimated interstellar reddening (Table 4) to the respective $EW/E(B - V)$ for field stars (Table 3) as well as subtracting the IS reddening contribution from the total observed reddening. The introduced uncertainties are quite large due to the scatter on the derived linear relationships (see above, Section 4.1). In particular IRAS 02229+6208 and IRAS 08544-443 require a correction for significant IS dust.

In the other direction, we can correct the IS-type stars (left panel of Figs. 7 to 15) by subtracting the CS (circumstellar) reddening contribution from the total reddening and the circumstellar $EW/E(B - V)$ (which we assume to be zero) from the observed EW . It shows then that all stars coincide neatly with the average Galactic relation. This is most noticeable for IRAS 17086-403 and IRAS 17395-0841 which have estimated CS contributions of 0.3 and 0.2 mag, respectively).

In principle, this result supports our initial interpretation that the DB carrier(s) may not be present in the circumstellar envelopes of post-AGB stars. However, strong variations from source to source are still visible in both groups of stars, which may be related to other observational properties of the shells not yet considered (Significant scatter is also observed for the sample of field stars; Sect. 4.1). Indeed, the results obtained suggest that some of the DB carriers could be completely absent in some of these envelopes while not in others.

4.5. DB strength vs. chemistry and spectral type

In order to explore whether other environmental conditions, like the dominant chemistry in the shell or the spectral type of the central star could also play a role in the differences observed between individual stars in the sample, we have further divided the two groups defined above in another four subgroups as a function of whether the chemistry of the shell is carbon-rich or oxygen-rich, or the spectra of the central star is of early-type (B-A)⁵ or of intermediate-type (F-G).

We do this because the dominant chemistry of the shell can completely determine the formation of specific compounds in the circumstellar shell. In oxygen-rich shells we expect to find aluminum oxides, amorphous or crystalline (fayalite, enstatite, forsterite, etc) silicates, water ice and other main constituents of oxygen-rich dust grains. In carbon-rich stars, instead, we can find carbon-based constituents, like chains or rings of carbon, graphite, hydrogenated amorphous carbon grains, fullerenes, nanodiamonds or PAHs.

⁵ Note that among the subgroup of early-type stars we have also included the few sources in Table 2 which are classified as planetary nebulae.

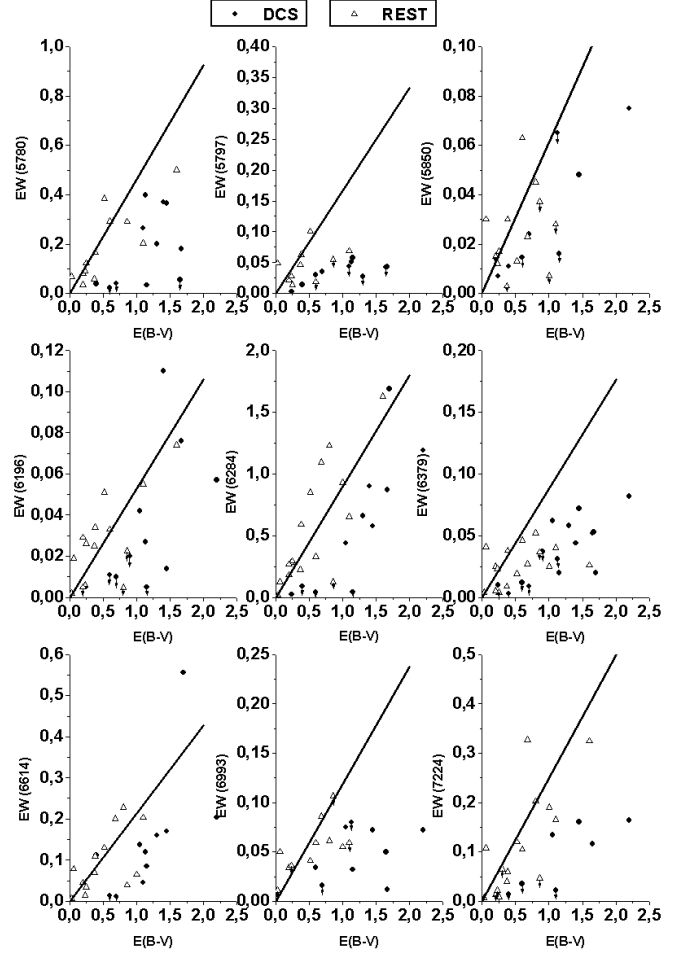


Fig. 6. Equivalent width of the 9 DBs selected for analysis as a function of $E(B - V)$ for the post-AGB stars in the sample in which filled circles represent the subsample of post-AGB stars dominated by circumstellar extinction (DCS-type) and open triangles the rest of stars in the sample. Solid lines again correspond to the fits derived in this paper for field stars dominated by interstellar extinction. The arrows indicate upper limits.

If a DB carrier had their origin in a compound or constituent related to only one of the above chemistries, we would expect to observe differences in strength from source to source as a function of their particular chemical composition.

On the other hand, it is also well known that the UV radiation field plays a crucial role in the processing of the circumstellar dust grains, not only immediately after they are formed, while they are still part of the shell, but also later when they are released to the ISM. Dust grains in the circumstellar envelopes of post-AGB stars are exposed to increasing doses of UV radiation due to the increasing effective temperature of the central star during its fast evolution towards the planetary nebula stage. First, when the central star is still showing late to intermediate spectral type, the UV radiation can be neglected, both as a consequence of the low effective temperature of the central star and because the higher density in the envelope during the early post-AGB stage would effectively protect (at least

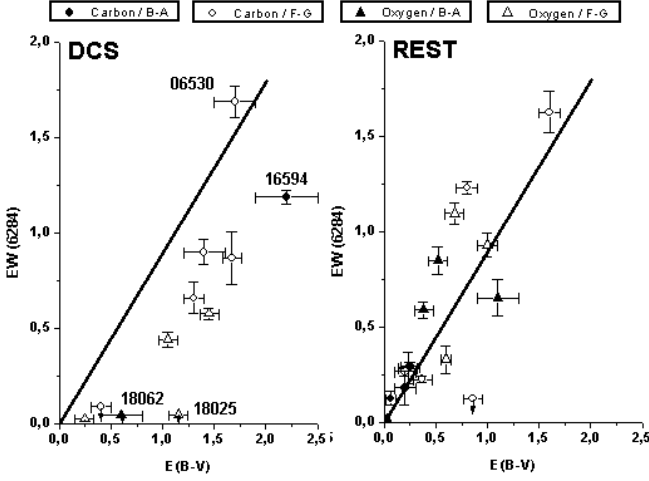


Fig. 7. Equivalent width of the 6284 Å band vs. $E(B - V)$ for the group of stars dominated by circumstellar extinction (left panel; DCS type) and for the rest of stars in the sample (right panel) with different symbols indicating the dominant chemistry and spectral type of the observed stars. The solid line represents the behaviour observed in field stars dominated by interstellar extinction, as deduced from the data shown in Figure 2.

temporarily) circumstellar dust grains from the energetic UV photons coming from the ISM. These conditions favour the formation of large dust grains which can survive in this less aggressive environment. Later in the post-AGB evolution the central stars become early-type and they start producing a considerable number of UV photons which may lead to an efficient processing of the dust grains in the shell, which in turn is less protected and more vulnerable also to the UV radiation field coming from the ISM. The combined effect of the UV photons coming from the central star and from the ambient ISM is expected to accelerate the processing of the dust grains, leading to new species like molecules, radicals (more or less complex) and other byproducts resulting from the partial or total evaporation of the grains, which will eventually be released to the ISM. Indeed, these byproducts could be the actual carriers of the DIBs commonly observed in the ISM.

If DB carriers are only related to the byproducts of the decomposition of these large circumstellar grains, we would expect to observe a deficit in DB strengths in post-AGB stars, only while the central stars are still showing a relatively low effective temperature.

Both effects can be combined, and it may also happen that the DB carriers are related to the byproducts of only a particular class of grains associated to a given dominant chemistry. In this case, we will be able to detect significant differences from source to source, both as a function of the spectral type of the central star as well as of the dominant chemistry in the shell.

In the next section we will analyse the influence of these environmental conditions (dominant chemistry and spectral type) on the observed results for each of the 9 DBs under study in our sample of post-AGB stars.

4.6. Analysis of individual bands

4.6.1. Analysis of the 6284 Å band

The 6284 Å band is not only the strongest ($EW/E(B - V) = 0.90$ Å/mag in the ISM) but also the broadest band included in our analysis. As such, it is relatively easy to measure, in spite of the contamination by telluric lines already shown in Figure 3, which must be carefully removed.

In Figure 7 we show the results obtained as a function of the dominant chemistry and of the spectral type of the central star for each of the two main subgroups identified in our sample.

The strength of the 6284 Å band as a function of $E(B - V)$ for the group of stars dominated by circumstellar extinction is presented in the left panel, while the results obtained for the rest of stars in our sample is shown in the right panel. As we can see, it is obvious that the post-AGB stars belonging to the DCS group show DB strengths systematically below those observed in the ISM (represented by the solid line).

Actually, in some cases this band is so weak than we can only determine an upper limit for its equivalent width. This is the case for IRAS 17436+5003 (oxygen-rich; F type), IRAS 18025-3906 (oxygen-rich; G type) and IRAS 18062+2410 (oxygen-rich; B type). It must be noted that the quality of the available spectra for these four stars is good enough to discard a non-detection which could be attributed to a poor signal-to-noise ratio.

Even for IRAS 16594-4656 (carbon-rich; B-type), the star with the second strongest feature in our sample, we find that the 6284 Å band is a factor of two weaker than expected for its high value of $E(B - V)$. This star is a well-known bipolar protoplanetary nebula which seems to be affected by a high internal extinction.

For IRAS 06530-0213 the band strength is typical for the total observed reddening being due to interstellar dust. On the other hand, the interstellar and circumstellar reddening contributions are estimated to be 1.3 and 0.4 mag, respectively (Sect. 4.3). Though this could indicate the presence of circumstellar DBs it should be noted that this line of sight lies in the galactic plane ($GLAT = -0.13$ degrees) and the interstellar reddening could be underestimated by the extinction model.

Remarkably, we find stars with a very weak band in all the subgroups, irrespective of the dominant chemistry and spectral type considered. This almost completely rules out the possibility of the 6284 Å band being generated in the circumstellar envelope of post-AGB stars, at least in the same proportion as in the ISM.

In contrast, in the right panel we can see that in general the rest of stars in the sample show a trend which is very similar to the one observed in the field stars in which the extinction is dominated by the interstellar contribution.

4.6.2. Analysis of the 5780 Å band

This DB has a $EW/E(B - V) = 0.46$ Å/mag in the ISM, so it is the second most intense after the 6284 Å band. In this particular case, it is important to remark that the spectral region corresponding to this band can be contaminated by the pres-

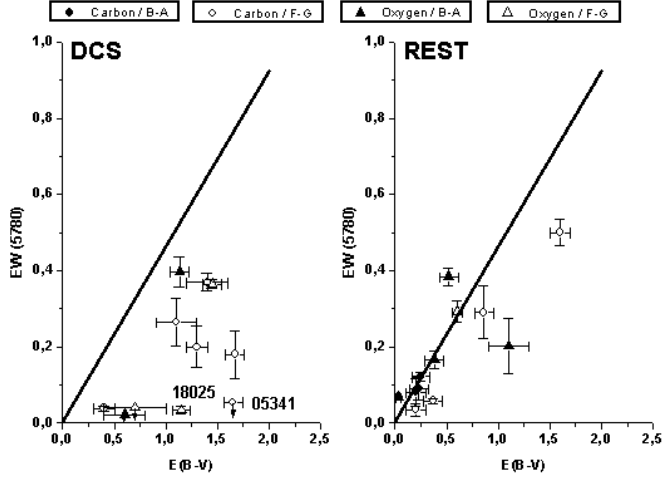


Fig. 8. Same as Figure 7, for the 5780 Å band.

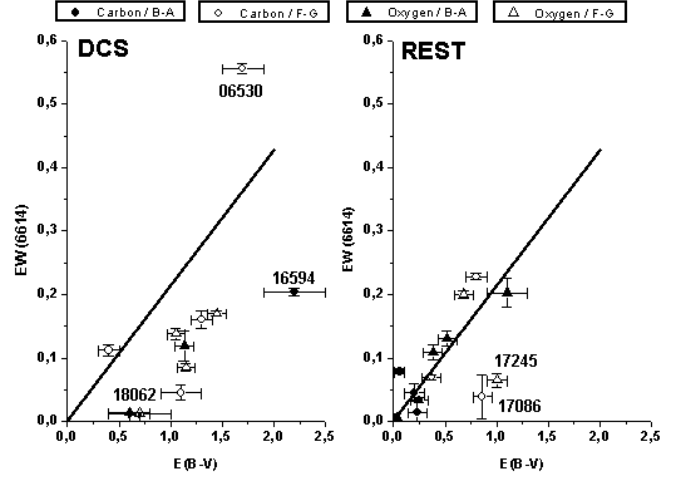


Fig. 10. Same as Figure 7, for the 6614 Å band.

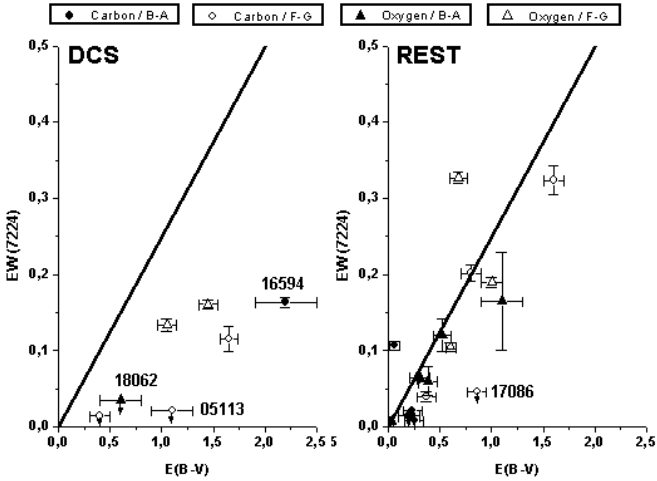


Fig. 9. Same as Figure 7, for the 7224 Å band.

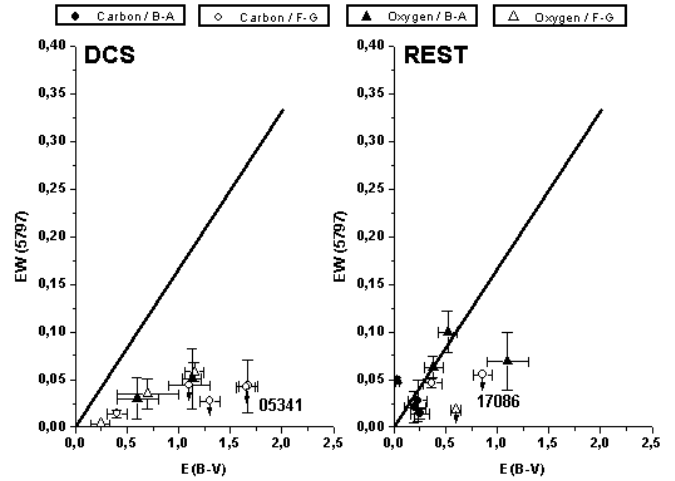


Fig. 11. Same as Figure 7, for the 5797 Å band.

ence of photospheric lines, which makes the evaluation of the band strength very difficult in stars with intermediate and late spectral types.

Note that to distinguish weak features from weak stellar lines or telluric contaminations is not always a simple task and makes it necessary to use detailed stellar models (to subtract the atmospheric features) and high resolution spectroscopy (to properly remove undesired contaminations), as the only way to derive the accurate strength of the band, which is beyond the scope of this work.

In Figure 8 we show the equivalent width of the 5780 Å band vs. $E(B-V)$ for each of the two main subgroups in which we have divided the sample. In the group of stars dominated by circumstellar extinction (left panel) we observe again strengths significantly weaker than those expected in stars for which the extinction is mainly of interstellar origin, represented by the solid line.

The non-detection of this DB in IRAS 05341+0852 (carbon-rich; F-type), despite the large value of $E(B-V)_{CS} \approx 1.5$ mag, is remarkable. This clearly suggests that the car-

rier of this band is completely absent at least in the envelopes of carbon-rich stars with intermediate spectral types. A similar conclusion can be derived for oxygen rich stars with intermediate spectral types from the very weak strength observed in IRAS 18025-3906 (oxygen-rich; B-type).

Unfortunately, the spectrum available for IRAS 16594-4656 does not cover the spectral range corresponding to this band, so we cannot extend the above conclusion to carbon-rich stars with earlier spectral types based on our data.

As in the case of the 6284 Å band, we can also observe in the right panel of Figure 8 that the rest of stars in the sample not identified as dominated by circumstellar extinction show a position in the diagram which is, overall, in better agreement with the results obtained for field stars in which the extinction is mainly of interstellar origin.

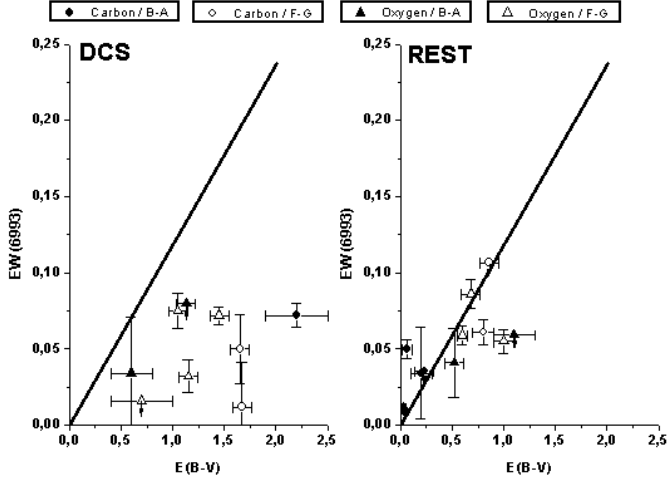


Fig. 12. Same as Figure 7, for the 6993 Å band.

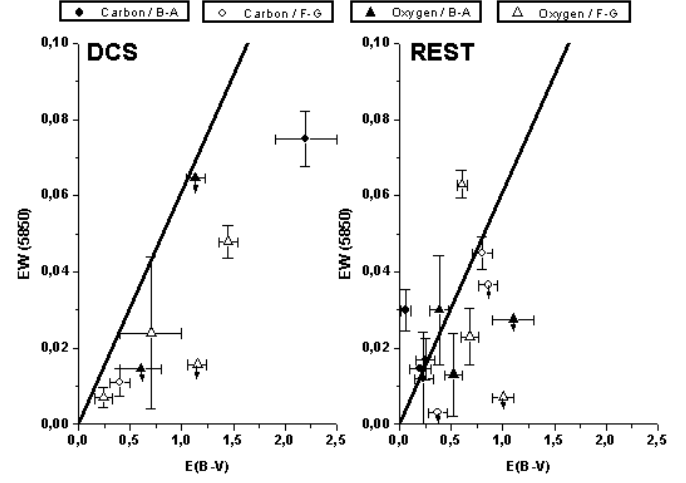


Fig. 14. Same as Figure 7, for the 5850 Å band.

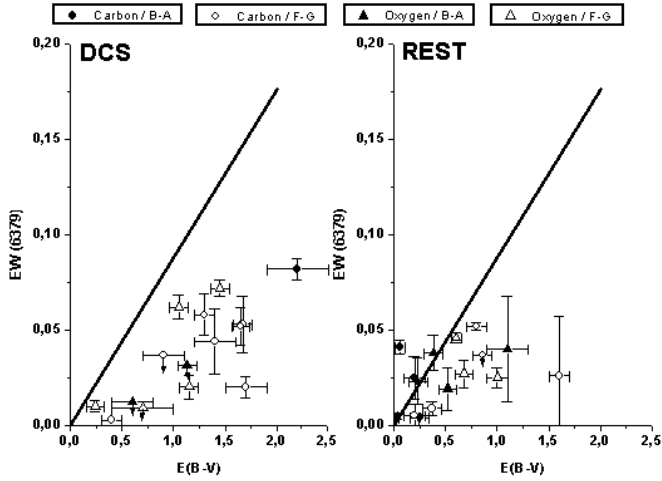


Fig. 13. Same as Figure 7, for the 6379 Å band.

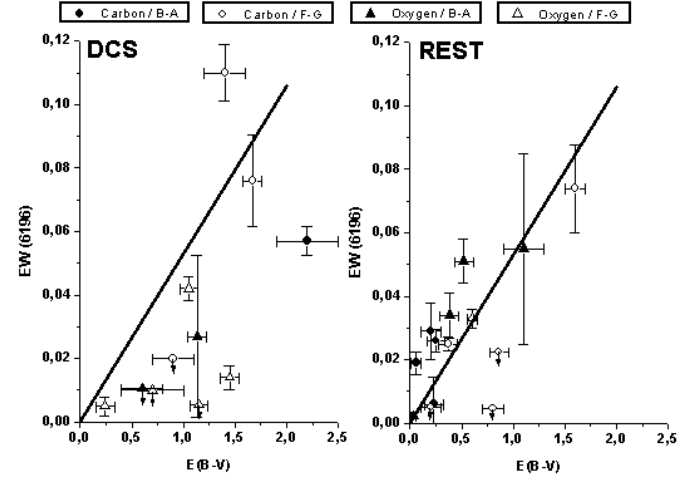


Fig. 15. Same as Figure 7, for the 6196 Å band.

4.6.3. Analysis of the 7224 Å band

This DB is not usually analysed in the literature because it is strongly affected by telluric contamination. As in the case of the 6284 Å band, we have carefully eliminated this contribution by dividing the normalised spectrum by the spectrum of the unreddened target HD 172324 (see Sect. 2).

In Figure 9 we show the equivalent width of the 7224 Å band vs. $E(B - V)$ for each of the two main subgroups identified in our sample. As for the two previous features, we find strengths which are much weaker than those measured in field stars in the subgroup formed by the stars in which the circumstellar contribution to the overall extinction is dominant (DCS; left panel). This again suggests that this band is not formed in the circumstellar envelope of post-AGB stars.

Again, the measured intensity of the 7224 Å band in IRAS 16594-4656 is rather weak and, once more, we find several non-detections: IRAS 05113+1347 (carbon-rich star) and IRAS 18062+2410. The latter case is remarkable because this is an oxygen-rich star with a B spectral type, where we have

neither detected the 6284 Å band. The non-detection of DBs in oxygen-rich envelopes around post-AGB stars indicates that the DB carriers are probably not generated in oxygen-rich environments. The absence of the band in the specific case of IRAS 18062+2410 suggests that they are neither produced even when the central star temperature is hot enough to produce high levels of UV irradiation on the (oxygen-rich) circumstellar grains.

For the rest of stars in the sample (Figure 9; right panel) we find again a behaviour which seems to follow very well the general trend observed in reference stars affected only by interstellar extinction. The exception is IRAS 17086-2403 (carbon rich star) for which we detect no DBs.

4.6.4. Analysis of the 6614 Å band

In Figure 10 we show the results of our analysis applied this time to the 6614 Å band.

In the left panel we show the equivalent widths measured in the subgroup of post-AGB stars dominated by circumstel-

lar extinction. As for the other bands, we see strengths which are systematically weaker than in the reference stars dominated by interstellar extinction, represented by the solid line in the diagram. The only non-detection in this case corresponds to IRAS 18062+2410, which we have previously pointed out as non-detected in the analysis made for the bands centred at 6284 and 7224 Å. The weak strength of this DB in IRAS 16594-4656 (carbon-rich, B type) is found to be again compatible with the absence of its carrier in the circumstellar envelope of this star, and confirms that the overall extinction affecting this source is the result of a quite similar contribution from the ISM and from the circumstellar material. The 6614 Å DB detected toward IRAS 06530-0213 is unusually strong for DBs in the DCS group and even with respect to the Galactic relationship. As mentioned earlier for the 6284 Å band toward the same target, this could point, for this particular source, towards the presence of circumstellar DBs or, perhaps more likely, an underestimation of the interstellar reddening.

For the rest of stars (right panel), as usual, we find that most of them are located in the region of the diagram corresponding to the field stars dominated by interstellar extinction. In this case, we would like to remark only the slightly discrepant position occupied by the oxygen-rich, F-type star IRAS 17245-3951 not yet previously identified as outlier in the above discussion. Again, the carbon rich star IRAS 17086-2403 shows very weak DBs.

4.6.5. Analysis of the 5797 Å band

This DB has been included in numerous studies in the literature because of its proximity to the nearby 5780 Å band. This has allowed a comparative analysis of their relative intensities in different astrophysical environments.

The 5797 Å band has a lower sensitivity to the extinction $EW/E(B - V) = 0.17$ Å/mag when it has been measured in the ISM, compared to the previous DBs. Similar to the adjacent 5780 Å band, it is necessary to take into account in our analysis the possible contamination due to the presence of atmospheric stellar lines in this spectral range in stars of intermediate and late spectral types, as it can affect our measurements.

In Figure 11 we show the equivalent width of this band vs. $E(B - V)$ as it has been measured from the available spectra for each subgroup of stars in which we have divided the sample. For stars in the DCS group (left panel), all post-AGB stars are found to show DB strengths which are considerably weaker than in the field stars, consistently with the results found in the other bands analysed so far.

Among the non-detections, we emphasize IRAS 05341+0852 (carbon-rich, F type) taking into account its large extinction $E(B - V)_{CS} = 1.5$ mag. We recall that this star was also found to show no indication of the presence of the accompanying feature at 5780 Å.

Unfortunately, the spectrum of IRAS 16594-4656 does not cover the wavelength corresponding to this DB (as it happened with the 5780 Å band).

In the right panel (rest sample) the line-of-sight toward IRAS 17086-2403 shows again a conspicuous absence of DBs.

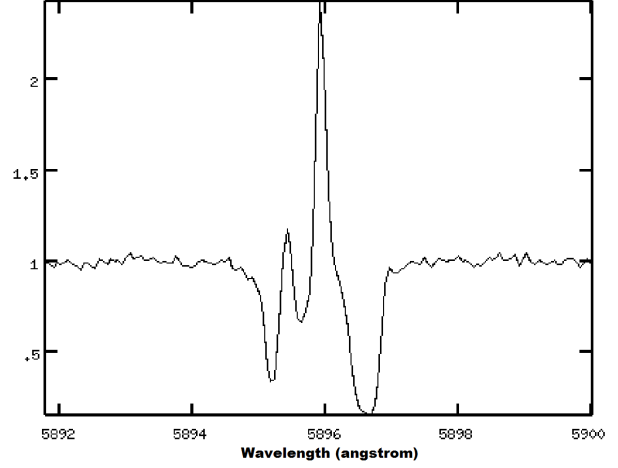


Fig. 16. The complex profile of the Na I D₁ line, as observed in IRAS 04296+3429.

4.6.6. Analysis of the 6993 Å band

This band is also among the ones not usually analysed in the literature, likely because of the presence of telluric lines in the spectral range adjacent to this band but also because of the intrinsic weakness of this DB, for which $EW/E(B - V) = 0.12$ Å/mag in the ISM.

In Figure 12 we show the results of our analysis for this DB for each of the subgroups in which we have divided the sample, again as a function of the dominant chemistry and the spectral type of the central star.

The results obtained are once more consistent with previous analysis performed for other DBs. We find a better agreement with the values obtained in reference stars dominated by interstellar extinction for the sources in the right panel, although in this case the effect is not so evident as in the previous analysis due to the larger errors associated to the measurements.

Consistent results, although more sensitive to measurement errors, are obtained when the features at 6379, 5850 and 6196 Å are analysed (see Figures 13, 14 and 15).

4.7. Radial velocity analysis

An additional way to check whether our conclusions are consistent with the available observational data is to analyse the Doppler velocities associated to the DBs detected in our stars.

The overall strategy consists of comparing these Doppler velocities with the radial velocities associated either to the atmospheric stellar absorptions or to the nebular and recombination emission lines sometimes detected in our spectra. In general, atmospheric and nebular lines are expected to match each other within the errors unless the central star is part of a binary system or the nebular shell shows a complex morphology.

If the DBs detected are formed in the circumstellar envelopes of these stars, we should measure Doppler velocities in these bands consistent with the characteristic radial velocities derived from the absorption and/or emission lines identified in the stellar spectra.

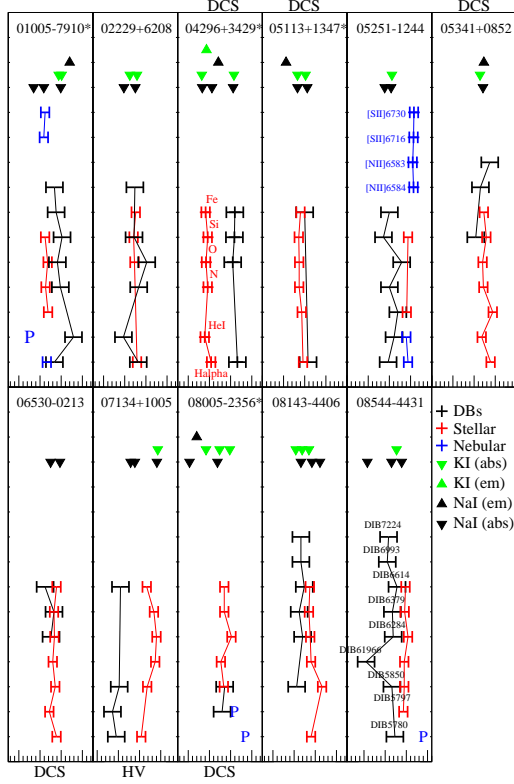


Fig. 17. Velocities of the DBs and the stellar and interstellar absorption lines and the nebular emission line components for each target are plotted per panel. The y-axis is in arbitrary units. The x-axis is the LSR velocity in km s^{-1} , with big tick-marks separated by 50 km s^{-1} . Note that the width of the panels are identical, i.e. 200 km s^{-1} , but the central velocity of each is shifted to show all lines for each target. Error bars are $\leq 10 \text{ km s}^{-1}$ for stellar lines, $\leq 20 \text{ km s}^{-1}$ for DBs and $\leq 5 \text{ km s}^{-1}$ for the sodium and potassium components. Targets dominated by circumstellar reddening are labeled ‘DCS’ and high radial velocity targets are labeled ‘HV’. The stellar and DB velocity components can be directly compared to those of neutral sodium and potassium in either emission (upward arrow) or absorption (downward arrow) plotted at the top of each panel.

In Table 6 (Online only) we give the radial velocities (in km s^{-1}), measured with respect to the Local Standard of Rest (LSR), associated to several atoms and ions, as derived from various atmospheric stellar absorptions and nebular emission lines identified in the stars of our sample. In addition, we also display the measurements made in $H\alpha$ at 6563 \AA and in the He I line at 6678 \AA . In the case of the atmospheric absorption lines shown in Table 6 the average velocity derived from several line measurements corresponding to various ions of the elements C, N, O, Si and Fe is presented. For the nebular lines, we have only considered the forbidden lines of $[\text{N II}]$ and $[\text{S II}]$, found around $H\alpha$. The typical uncertainties are of the order of $5\text{--}10 \text{ km s}^{-1}$.

In addition, in Table 7 (Online only) we present the velocities derived from the analysis of the Na I D (5889.95 and 5895.92 \AA) doublet and of the K I (7698.97 \AA) line, which are in most cases also well detected in our spectra (uncertainties

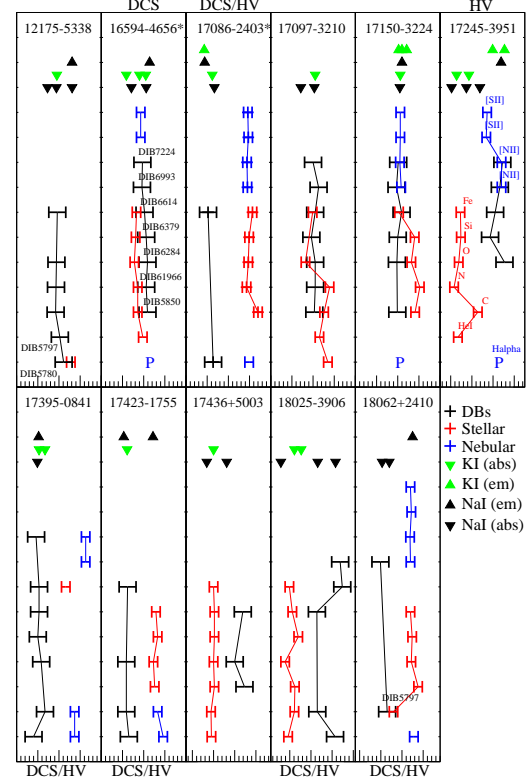


Fig. 17. (continued).

are ~ 3 to 5 km s^{-1}). These lines, like the DBs that we want to analyse, usually originate in the ISM, but they can also form in the circumstellar shell. In this case, the circumstellar component usually appears in emission over the interstellar absorption (see Figure 16). In general, these lines show very complex absorption profiles as they reflect the different velocities of the clouds located along the line of sight. In some of our stars the circumstellar component may contribute significantly to the observed profile and can be used as a further test to identify the origin of analogue velocity components which may be present in our favourite DB.

Table 8 (Online only) shows the radial velocities associated to the DBs observed in the stars of our sample, which can then be compared to the velocities provided in Tables 6 and 7.

It is important to take into account that deriving velocities for DBs is in many cases a complicated task, especially if the features under analysis are weak in strength. In general, the Doppler shift measurements are determined by assuming that the absorption peak is a good approximation to the centre of the feature. We estimate that, on average, the errors in Table 8 may be affected by errors of the order of $10\text{--}20 \text{ km s}^{-1}$.

Comparing Tables 6 and 7 we observe that in most cases there is at least one velocity component associated to the sodium doublet or the potassium line, either in emission or in absorption, that can be interpreted as having a stellar or circumstellar origin. The circumstellar nature of these lines is easy to determine when they are found in emission. The radial velocities measured in this case are usually coincident with the systemic velocity of the post-AGB star. The few cases found in which our measurements do not support this statement are indi-

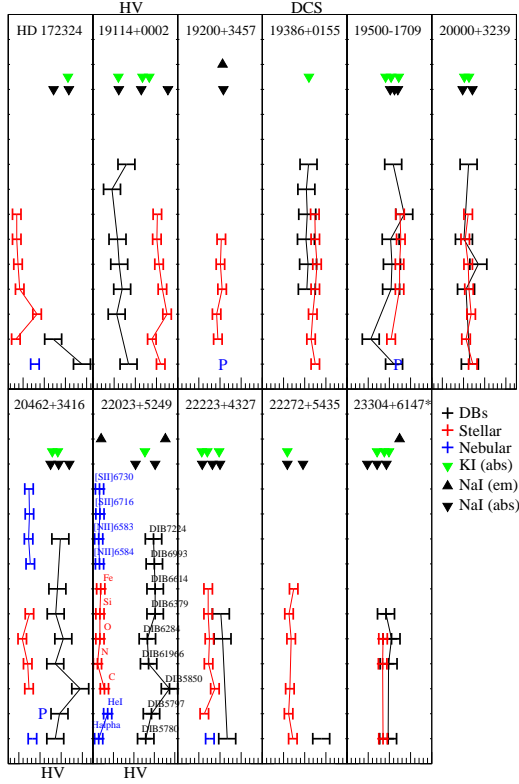


Fig. 17. (continued).

cated with an asterisk in Table 7 and Fig. 17. They correspond to very complex Na I D line profiles in which the circumstellar emission appears over-imposed to the interstellar absorption.

Figure 17 shows, for ease of comparison, the velocities of the DBs and the (inter-)stellar absorption and emission components for each target. For the majority of the targets these graphs show consistent velocities for the stellar lines. DB velocities are also consistent with each other. For several cases the nebular (emission) lines are significantly shifted with respect to the atmospheric lines (*e.g.* IRAS 17245-3951) due to binarity of the system and/or a complex wind structure. These stellar and DB velocity components can be directly compared to those of neutral sodium and potassium in the respective line-of-sight.

If DB carriers are present in the circumstellar envelopes of some of the post-AGB stars in our sample, we would expect to find as well matches between the velocities shown in Table 8 and those in Table 6 (see Figure 18), especially for those stars in which we have detected circumstellar Na I in emission belonging to the DCS group. Remarkably, in not any case we find values consistent with the velocities associated to the DBs which cannot be explained as a natural consequence of interstellar clouds with a similar velocity present in the line of sight.

The inconsistency between velocities is more obvious if we have a look at those stars showing very high radial velocities (HV in Table 4 and Fig. 17). Several of the HV targets have radial velocities larger than 100 km s^{-1} . Such large velocity differences are comparable to those measured for successfully detected extra-galactic DBs (Ehrenfreund et al 2002; Cox et al. 2007).

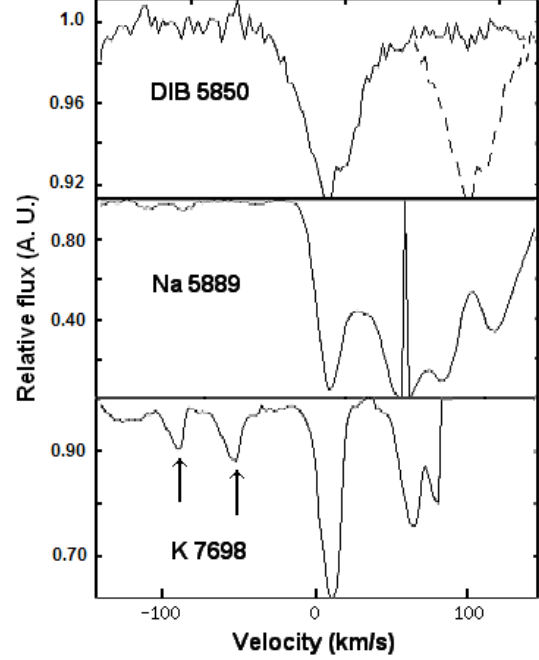


Fig. 18. The 5850 Å band observed in the high radial velocity ($\sim 100 \text{ km s}^{-1}$) sample star IRAS 19114+0002 (solid line). The non-detection of this feature at the Doppler-shifted velocity corresponding to the central star (dashed line) confirms the interstellar nature of the band and the absence of a circumstellar component. The potassium and sodium velocity structures are shown in the bottom panels in order to illustrate the distribution of interstellar medium in this line of sight. A narrow sodium emission line is seen in the middle panel. The two arrows in the bottom most panel indicate two telluric features next to the potassium line.

In the top panel of Fig. 18 we illustrate the radial velocities difference expected between the interstellar (solid line) and circumstellar (dashed line) DBs for the HV target IRAS 19114+0002. The narrow 5850 Å CS DB (shifted to the stellar radial velocity) would be well separated from the observed (IS) DB. The atomic line profiles of sodium (middle panel) and potassium (bottom panel) are shown to indicate the ISM distribution in this line of sight. Note also the narrow sodium emission.

In none of the stars is it possible to assign DBs to nebular or stellar lines exclusively. This strongly supports our conclusion that the DBs detected toward the post-AGB stars in our sample are not originated in their circumstellar envelopes.

Globally considered, the radial velocity analysis here presented gives more strength to our proposed scenario, in which the DB carriers are suggested to be not present in the circumstellar envelopes of post-AGB stars, or at least not under the excitation conditions necessary to produce the transitions that we identify as DBs in the ISM. Targets that show large velocity differences between interstellar and circumstellar lines and that show significant circumstellar reddening (*e.g.* IRAS 17086-2403, IRAS 17423-1755, IRAS 18025-3906 and IRAS 18062+2410) provide the best candidates to search for

the presence of (weak) circumstellar DBs separated from the interstellar DBs. Our current spectra are of insufficient quality to search for these weak features next to the observed DIBs. Note that both CS and IS DBs could coexist. And, if separated by more than their FWHM ($\sim 40 - 60 \text{ km s}^{-1}$ for narrow DBs) the central velocity of the IS and (possibly) CS DB would not be affected by each other.

5. Conclusions

The equivalent widths of 9 DBs commonly found in the ISM have been determined for a representative sample of galactic post-AGB stars displaying a wide variety of observational properties. We present here the results of our extensive survey to look for DBs in envelopes of evolved stars.

We have carefully disentangled the observed extinction by assessing the expected interstellar extinction for each of the observed targets. This allowed us to select a sub-sample of targets whose line of sight reddenings are dominated ($> 50\%$) by circumstellar dust.

In general, the strengths of the DBs are found to follow the same correlation with $E(B - V)$ observed in field stars only in those sources showing little circumstellar contribution to the overall reddening. In contrast, DBs are weak or absent in sources dominated by circumstellar reddening, irrespective of the dominant chemistry and spectral type of the central star, although our conclusions should be taken with caution due to the relatively small sample size.

The results obtained suggest that the carrier(s) of the DBs do not form or at least they are not “available” to produce any detectable spectral feature during the post-AGB phase. The carriers, if present in the circumstellar envelope of these stars are not found under the environmental conditions needed to excite the transitions which we identify as DBs in the ISM.

The radial velocity analysis of the features observed in individual sources confirm this result, as the Doppler shifts measured are always found to be consistent with an interstellar origin for the bands observed.

DB carriers may be carbonaceous species or radicals attached to large organic molecules, trapped in lattice or more complex structures, or constituents of the mantle of circumstellar dust grains which are liberated to the ISM only after strong UV irradiation (either UV photons from the central star or from the more energetic interstellar UV field).

In this sense, the identification of the carriers as strongly ionised PAHs and/or radicals liberated from carbonaceous species as a consequence of photo-evaporation of dust grains in the ISM looks tempting and would be consistent with our observations.

However, we do not find any evidence of the carbonaceous nature of the carrier(s) in our sample stars, something generally accepted in the literature, nor any correlation with the presence of PAHs in the mid-infrared spectrum of these sources, as it has been claimed by several authors in the past.

If DBs are connected with PAHs or with any other carbonaceous species such as the ones suggested in the introduction of this paper, their carrier(s) must form at a later stage, probably under different excitation conditions, once the envelope of the

post-AGB star is totally diluted in the interstellar medium as a result of the expansion of the shell.

Acknowledgements. Many of the spectra used in the analysis here presented were kindly provided by Hans van Winckel and Maarten Reyniers, working at the Katholieke Universiteit Leuven, Belgium. The authors are also grateful to Bernard Foing and Nathalie Boudin, who participated in the early stage of this project and with whom we had very fruitful discussions. We sincerely thank the referees for their helpful and constructive comments. This work was partially funded by grants AYA2003-09499 and AYA2004-05382 of the Spanish Ministerio de Ciencia y Tecnología.

References

- Allamandola, L.J., Hudgins, D.M., & Sandford, S.A. 1999, *ApJ*, 511, L115
- Arellano, A., Giridhar, S., & Mathias, P. 2001, *A&A*, 368, 250
- Arkhipova, V.P., Ikonnikova, N., Noskova, R., & Sokol, G. 2000, *AstL*, 26, 609
- Bakker, E.J., Dishoeck, E.F.V., Waters, L.B.F.M., & Schoenmaker, T. 1997, *A&A*, 323, 469
- Bujarrabal, V., Alcolea, J., & Planesas, P. 1992, *A&A*, 257, 701
- Clube, K.L., & Gledhill, T.M. 2004, *MNRAS*, 355, 17
- Cohen, M., & Jones, B.F. 1987, *ApJ Letters*, 321, 151
- Cox, N.L.J., Kaper, L., Foing, B. H., & Ehrenfreund, P. 2005, *A&A*, 438, 187
- Cox, N.L.J., Cordiner, M.A., Ehrenfreund, P., et al. 2007, *A&A*, 470, 941
- Crawford, M.K., Tielens, A.G.G.M., & Allamandola, L.J. 1985, *ApJ Letters*, 293, 45
- Desmurs, J., Baudry, A., Sivagnanam, P., & Henkel, C. 2002, *A&A*, 394, 975
- Douglas, A.E. 1977, *Nature*, 269, 130
- Drimmel, R., Cabrera-Lavers, A., & López-Corredoira, M. 2003, 409, 205
- Ehrenfreund, P., & Foing, B.H. 1996, *A&A Letters*, 307, 25
- Ehrenfreund, P., Cami, J., Jimnez-Vicente, J., Foing, B. H., Kaper, L., van der Meer, A., Cox, N., d’Hendecourt, L., Maier, J. P., Salama, F., Sarre, P. J., Snow, T. P., Sonnentrucker, P., *ApJ Letters*, 576, 117
- Fernie, J.D. 1983, *ApJ Supplements*, 52, 7
- Fitzgerald, M.P. 1970, *A&A*, 4, 234
- Foing, B.H., & Ehrenfreund, P. 1994, *Nature*, 369, 296
- Fujii, F., Nakada, Y., & Parthasarathy, M. 2002, *A&A*, 385, 884
- Fulara, J., & Krelowski, J. 2000, *New Astronomy Reviews*, 44, 581
- Galazutdinov, G.A., Musaev, F.A., Krelowski, J., & Walker G.A.H. 2000, *PASP*, 112, 648
- Galazutdinov, G.A., Stachowska, W., Musaev, F.A., et al. 2002, *A&A*, 396, 987
- García-Lario, P., Manchado, A., Pych, W., & Pottasch, S.R. 1997a, *A&A Suppl. Ser.*, 126, 479
- García-Lario, P., Manchado, A., Ulla, A., & Manteiga, M. 1999, *ApJ*, 513, 941
- García-Lario, P., Parthasarathy, M., de Martino, D., et al. 1997b, *A&A*, 326, 1103
- Gauba, G., & Parthasarathy, M. 2003, *A&A*, 407, 1007
- Gauba, G., & Parthasarathy, M. 2004, *A&A*, 417, 201

- Gauba, G., Parthasarathy, M., Kumar, B., Yadav, R.K.S., & Sagar, R. 2003, *A&A*, 404, 305
- Guarinos, J. 1988a, *Bull. d'inf. cent. données stellaires*, 35, 161
- Guarinos, J. 1988b, *Bull. d'inf. cent. données stellaires*, 34, 141
- Guarinos, J. 1997, *VizieR On-line Data Catalog: II/135*. <http://vizier.u-strasbg.fr/viz-bin/VizieR>
- Heap, S.R., & Augensen, H.J. 1987, *ApJ*, 313, 286
- Heger, M.L. 1922, *Lick Observatory bulletin*, 337, 141
- Herbig, G.H. 1995, *ARA&A*, 33, 19
- Herbig, G.H. 1993, *ApJ*, 407, 142
- Hrivnak, B.J. 1995, *ApJ*, 438, 341
- Hrivnak, B.J., & Kwok, S. 1991, *ApJ*, 371, 631
- Hrivnak, B.J., & Kwok, S. 1999, *ApJ*, 513, 869
- Hrivnak, B.J., & Reddy, B.E. 2003, *ApJ*, 590, 1049
- Hrivnak, B.J., Kwok, S., & Su, K.Y.L. 1999, *ApJ*, 524, 849
- Hrivnak, B.J., Kwok, S., & Volk, K. 1989, *ApJ*, 346, 265
- Hrivnak, B.J., Volk, K., & Kwok, S. 2000, *ApJ*, 535, 275
- Hu, J.Y., Slijkhuis, S., de Jong, T., & Jiang, B.W. 1993a, *A&A Supplements*, 100, 413
- Hu, J.Y., Slijkhuis, S., Nguyen-Q-Rieu, & de Jong, T. 1993b, *A&A*, 273, 185
- Hu, J.Y., te Lintel Hekkert, P., Slijkhuis, F., et al. 1994, *A&A Supplements*, 103, 301
- Iglesias-Groth, S. 2004, *Lecture Notes and Essays in Astrophysics I*, 105
- Iglesias-Groth, S. 2007, *ApJ Letters*, 661, 167
- Jenniskens, P., & Désert, F. 1994, *A&A Supplements*, 106, 39
- Kendall, T.R., Maun, N., McCombie, J., & Sarre, P.J. 2002, *A&A*, 387, 624
- Kerr, T.H., Hibbins, R.E., Fossey, S.J., Miles, J.R., & Sarre, P.J. 1998, *ApJ*, 495, 941
- Klochkova, V.G., Szczerba, R., Panchuk, V.E., & Volk, K. 1999, *A&A*, 345, 905914
- Klochkova, V.G., Szczerba, R., & Panchuk, V.E. 2000, *AstL*, 2, 88103
- Klochkova, V.G., Yushkin, M.V., Miroshnichenko, A.S., Panchuk, V.E., & Bjorkman, K.S. 2002, *A&A*, 392, 143
- Krelowski, J., & Walker, G.A.H. 1987, *ApJ*, 312, 860
- Krelowski, J., Galazutdinov, G.A., & Musaev, F.A. 1998, *ApJ*, 493, 217
- Krelowski, J., Schmidt, M., & Snow, T.P. 1997, *PASP*, 109, 1135
- Kwok, S., Hrivnak, B.J., & Geballe, T.R. 1995, *ApJ*, 454, 394
- Kwok, S., Volk, K., & Hrivnak, B.J. 1999, *IAU Symp.*, 191, 297
- Le Bertre, T. 1990, *A&A*, 236, 472
- Le Bertre, T., & Lequeux, J. 1992, *A&A*, 255, 288
- Le Bertre, T., & Lequeux, J. 1993, *A&A*, 274, 909
- Leger, A., & D'Hendecourt, L. 1985, *A&A*, 146, 81
- Lewis, B.M. 2000, *ApJ*, 533, 959
- Maas, T., van Winckel, H., Evans, T.L., et al. 2003, *A&A*, 405, 271
- Malfait, K., Bogaert, E., & Waelkens, C. 1998, *A&A*, 331, 211
- Maun, N., & Kendall, T.R. 2004, *A&A*, 428, 535
- McCall, B.J., Oka, T., Thorburn, J., Hobbs, L., & York, D.G. 2002, *ApJ*, 567, 145
- Megier, A., Krelowski, J., & Weselak, T. 2005, *MNRAS*, 358, 563
- Meixner, M., Ueta, T., Dayal, A., et al. 1999, *ApJ Supplements*, 122, 221
- Merrill, P.W. 1936, *ApJ*, 83, 126
- Neckel, T., Klare, G., & Sarcander, M. 1995, *VizieR Online Data Catalog*, 2062
- Oudmaijer, R.D., van der Veen, W.E.C.J., Waters, L.B.F.M., et al. 1992, *A&A Supplements*, 96, 625
- Parthasarathy, M., García-Lario, P., Sivarania, T., Manchado, A., & Sanz Fernández de Córdoba, L.. 2000a, *A&A*, 357, 241
- Parthasarathy, M., Vijapurkar, J., & Drilling, J.S. 2000b, *A&A Supplements*, 145, 269
- Pottasch, S.R., Bernard-Salas, J., Beintema, D.A., & Feibelman, W.A. 2004, *A&A*, 423, 593
- Prichet, C.J., & Grillmair, C.J. 1984, *PASP*, 96, 349
- Reddy, B.E., & Parthasarathy, M. 1996, *AJ*, 112, 2053
- Reddy, B.E., Bakker, E.J., & Hrivnak, B.J. 1999, *ApJ*, 524, 831
- Reed, B.C., & Vance, S.J. 1996, *AJ*, 112, 2855
- Reyniers, M., van Winckel, H., Gallino, R., & Straniero, O. 2004, *A&A*, 417, 269
- Ruiterkamp, R., Cox, N.L.J., Spaans, M., et al. 2005, *A&A*, 432, 515
- Salama, F., Galazutdinov, G.A., Krelowski, J. et al. 1999, *ApJ*, 526, 265
- Salama, F., Bakes, E.L.O., Allamandola, L.J., & Tielens, A.G.G.M. 1996, *ApJ*, 458, 621
- Sarre, P.J., Miles, J.R., Kerr, T.H., et al. 1995, *MNRAS Letters*, 277, 41
- Sarre, P.J. 2006, *Journal of Molecular Spectroscopy*, 238, 1
- Scarrott, S.M., Watkin, S., Miles, J.R., & Sarre, P.J. 1992, *MNRAS short communication*, 255, 11
- Snow, Jr., T.P., & Wallerstein, G. 1972, *PASP*, 84, 492
- Snow, Jr., T.P. 1973, *PASP*, 85, 590
- Suárez, O. 2004, PhD Thesis, Universidade de Vigo, Spain
- Suárez, O., García-Lario, P., Manchado, A., Manteiga, M., Ulla, A. & Pottasch, S. R. 2006, *A&A*, 458, 173
- te Lintel Hekkert, P., Caswell, J.L., Habing, H.J., Haynes, R.F., & Norris, R.P. 1991, *A&A Supplements*, 90, 327
- Thorburn, J.A., Hobbs, L.M., McCall, B.J., et al. 2003, *ApJ*, 584, 339356
- Torres-Peimbert, S., Peimbert, M., & Daltabuit, E. 1980, *ApJ*, 238, 133
- Turner, D.G., & Drilling, J.S. 1984, *PASP*, 96, 292
- Van de Steene, G.C.V., & van Hoof, P. 2003, *A&A*, 406, 773
- Van der Veen, W.E.C.J., Habing, H.J., & Geballe, T.R. 1989, *A&A*, 226, 108
- Van der Zwet, G.P., & Allamandola, L.J. 1985, *A&A*, 146, 76
- Van Winckel, H.. 1997, *A&A*, 319, 561
- Van Winckel, H., & Reyniers, M. 2000, *A&A*, 354, 135
- Volk, K., & Kwok, S. 1989, *ApJ*, 342, 345
- Waters, L.B.F.M., Lamers, H.J.G.L.M., Snow, T.P., et al 1989, *A&A*, 211, 208
- Weselak, T., Fulara, J., Schmidt, M.R., & Krelowski, J. 2001, *A&A*, 377, 677
- Woodsworth, A. W., Kwok, S., & Chan, S. J. 1990, 228, 503
- Zács, L., Schmidh, M.R., & Szczerba, R. 1999, *MNRAS*, 306, 903

- Začs, L., Schmidh, M.R., Szczerba, R. & Spēlmanis, R. 1999, ASPC, 188, 221
- Začs, L., Spēlmanis, R., Schmidh, M.R., & Szczerba, R. 2001, ASP Conference Series, 223, 1645
- Začs, L., Spēlmanis, R., Musaev, F. A., & Galazutdinov, G. A. 2003, MNRAS, 339, 460

Online Material

Table 5. Equivalent width measurements (in Å) corresponding to the 9 DBs analysed in our sample of post-AGB stars.

IRAS Name	<i>EW</i> (Å)								
	5780	5797	5850	6196	6284	6379	6614	6993	7224
01005+7910	0.08 ± 0.04	0.021 ± 0.009	≤ 0.01	0.029 ± 0.009	0.18 ± 0.09	0.025 ± 0.009	0.045 ± 0.009	0.034 ± 0.009	≤ 0.01
02229+6208	0.18 ± 0.06	0.043 ± 0.009	?	0.076 ± 0.009	0.87 ± 0.09	0.053 ± 0.009	?	0.012 ± 0.009	?
04296+3429	0.20 ± 0.06	≤ 0.03	—	?	0.66 ± 0.08	0.058 ± 0.009	0.16 ± 0.01	—	?
05113+1347	0.27 ± 0.06	≤ 0.04	?	?	?	?	0.045 ± 0.009	—	≤ 0.02
05251–1244	0.09 ± 0.03	0.028 ± 0.009	0.012 ± 0.009	0.006 ± 0.009	0.28 ± 0.08	0.023 ± 0.009	0.014 ± 0.009	≤ 0.04	≤ 0.02
05341+0852	≤ 0.06	≤ 0.04	—	?	?	0.052 ± 0.009	?	0.050 ± 0.009	0.12 ± 0.02
06530–0213	—	—	?	?	1.69 ± 0.08	0.020 ± 0.006	0.556 ± 0.008	—	—
07134+1005	0.039 ± 0.006	0.014 ± 0.004	0.011 ± 0.004	?	≤ 0.09	≤ 0.003	0.112 ± 0.009	—	≤ 0.01
08005–2356	≤ 0.04	0.035 ± 0.009	0.024 ± 0.009	≤ 0.01	?	≤ 0.009	≤ 0.01	≤ 0.02	?
08143–4406	—	—	0.045 ± 0.004	≤ 0.005	1.23 ± 0.03	0.052 ± 0.002	0.228 ± 0.005	0.061 ± 0.008	0.202 ± 0.009
08544–4431	0.37 ± 0.01	?	0.048 ± 0.004	0.014 ± 0.004	0.58 ± 0.03	0.072 ± 0.004	0.170 ± 0.003	0.072 ± 0.006	0.161 ± 0.007
12175–5338	0.12 ± 0.01	0.014 ± 0.006	0.017 ± 0.005	0.026 ± 0.004	0.29 ± 0.02	≤ 0.004	0.034 ± 0.004	—	≤ 0.008
16594–4656	—	—	0.075 ± 0.007	0.057 ± 0.005	1.19 ± 0.04	0.082 ± 0.006	0.204 ± 0.007	0.072 ± 0.008	0.164 ± 0.007
17086–2403	0.29 ± 0.07	≤ ± 0.06	≤ 0.04	≤ 0.02	≤ 0.1	≤ 0.04	0.04 ± 0.03	≤ 0.1	≤ 0.05
17097–3210	—	—	0.030 ± 0.006	0.019 ± 0.004	0.13 ± 0.04	0.041 ± 0.004	0.079 ± 0.005	0.050 ± 0.006	0.107 ± 0.006
17150–3224	—	—	0.023 ± 0.007	?	1.10 ± 0.06	0.027 ± 0.007	0.200 ± 0.006	0.086 ± 0.009	0.327 ± 0.007
17245–3951	—	—	≤ 0.007	?	0.93 ± 0.06	0.025 ± 0.006	0.065 ± 0.009	0.055 ± 0.008	0.190 ± 0.007
17395–0841	0.20 ± 0.07	0.07 ± 0.03	≤ 0.03	0.06 ± 0.03	0.65 ± 0.09	0.040 ± 0.009	0.20 ± 0.02	≤ 0.06	0.165 ± 0.065
17423–1755	0.40 ± 0.04	0.05 ± 0.03	≤ 0.06	0.027 ± 0.009	?	≤ 0.03	0.12 ± 0.02	≤ 0.08	?
17436+5003	?	≤ 0.003	0.007 ± 0.003	0.005 ± 0.003	≤ 0.02	0.010 ± 0.003	?	—	?
18025–3906	0.034 ± 0.009	0.058 ± 0.009	≤ 0.02	≤ 0.005	≤ 0.05	0.020 ± 0.006	0.085 ± 0.007	0.032 ± 0.009	?
18062+2410	? 0.02	0.03 ± 0.02	≤ 0.01	≤ 0.01	≤ 0.04	≤ 0.01	≤ 0.01	0.034 ± 0.009	≤ 0.04
HD 172324	0.068 ± 0.004	0.049 ± 0.004	?	≤ 0.002	≤ 0.02	≤ 0.004	≤ 0.006	≤ 0.01	≤ 0.007
19114+0002	0.29 ± 0.03	≤ 0.02	0.063 ± 0.004	0.033 ± 0.003	0.33 ± 0.07	0.046 ± 0.002	?	0.059 ± 0.006	0.105 ± 0.006
19200+3457	?	?	?	?	?	?	?	?	≤ 0.07
19386+0155	—	—	—	0.042 ± 0.004	0.44 ± 0.04	0.062 ± 0.006	0.138 ± 0.009	0.075 ± 0.009	0.134 ± 0.008
19500–1709	0.058 ± 0.006	0.046 ± 0.004	≤ 0.003	0.025 ± 0.002	0.23 ± 0.02	0.009 ± 0.004	0.069 ± 0.004	—	0.040 ± 0.007
20000+3239	0.50 ± 0.03	?	?	0.074 ± 0.009	1.63 ± 0.09	0.026 ± 0.009	?	—	0.32 ± 0.02
20462+3416	0.16 ± 0.02	0.063 ± 0.009	0.030 ± 0.009	0.034 ± 0.007	0.59 ± 0.04	0.038 ± 0.009	0.109 ± 0.009	—	0.06 ± 0.02
22023+5249	0.38 ± 0.02	0.10 ± 0.02	0.013 ± 0.009	0.051 ± 0.007	0.85 ± 0.07	0.019 ± 0.009	0.130 ± 0.009	0.041 ± 0.009	0.12 ± 0.02
22223+4327	0.035 ± 0.009	?	?	≤ 0.005	0.27 ± 0.03	0.005 ± 0.006	?	—	?
22272+5435	?	?	?	≤ 0.02	?	≤ 0.04	?	—	?
23304+6147	0.37 ± 0.02	?	?	0.110 ± 0.009	0.90 ± 0.07	0.044 ± 0.009	?	—	?

?: contamination by atmospheric stellar lines or poor S/N; —: spectral range not covered.

Table 6. Radial velocity measurements (in km s⁻¹) associated to several atmospheric stellar and nebular lines detected in the post-AGB stars of our sample.

IRAS Name	H α 6563	He I 6678	C	N	O	Si	Fe	[N II] 6548	[N II] 6583	[S II] 6716	[S II] 6730
01005+7910	-34 e	-76 P	-31	-37	-32	-38	—	—	—	-41	-38
02229+6208	29 a	—	—	—	23	21	26	—	—	—	—
04296+3429	4 a	-11 a	—	-4	-8	-4	-9	—	—	—	—
05113+1347	-4 a	—	-7	-13	-13	-14	-10	—	—	—	—
05251-1244	44 e	40 e	41	—	—	44	—	32, 57	31, 55	31, 57	32, 58
05341+0852	39 a	18 a	44	22	20	29	23	—	—	—	—
06530-0213	39 a	22 a	36	30	34	33	39	—	—	—	—
07134+1005	54 a	—	68	87	90	84	67	—	—	—	—
08005-2356	85 P	59 P	34	27	52	35	35	—	—	—	—
08143-4406	40 a	—	66	40	38	35	37	—	—	—	—
08544-4431	90 P	43 a	45	45	54	46	48	—	—	—	—
12175-5338	28 a	—	—	—	—	—	—	—	—	—	—
16594-4656	15 P	-2 a	-14	-14	-22	-19	-17	—	—	-7	-7
17086-2403	99 e	—	120	93	97	99	107	95	94	97	96
17097-3210	35 a	15 a	26	39	-18	—	-1	—	—	—	—
17150-3224*	5 P	—	41	52	32	40	3	8	5	6	6
17245-3951*	14 P	-83 a	-36	-92	-81	-76	-77	20	20	-16	-14
17395-0841	87 e	87 e	—	—	—	—	66	113	113	—	—
17423-1755	96 e	83 e	76	73	83	79	—	—	—	—	—
17436+5003	-55 a	-56 a	-48	-50	-48	-48	-50	—	—	—	—
18025-3906	-104 a	-89 a	-88	-111	-80	-94	-101	—	—	—	—
18062+2410	78 e	30 a	88	72	74	70	—	70	69	72	70
HD 172324	-72 e	-117 a	-67	-108	-112	-115	-115	—	—	—	—
19114+0002	110 a	89 a	125	114	106	101	102	—	—	—	—
19200+3457	7 P	-5 a	-8	5	1	3	—	—	—	—	—
19386+0155	25 a	15 a	19	25	29	25	24	—	—	—	—
19500-1709	20 P	4 a	—	24	24	27	25	—	—	—	—
20000+3239	22 a	6 a	18	13	11	4	11	—	—	—	—
20462+3416	-68 e	-44 P	-76	-79	-92	-75	—	-73	-77	-75	-76
22023+5249	-136 e	-114 e	-122	-139	-133	-133	-131	-134	-136	-133	-134
22223+4327	-24 e	-37 a	-12	-27	-25	-28	-28	—	—	—	—
22272+5435	-28 a	-38 a	-35	—	-32	-37	-26	—	—	—	—
23304+6147	-15 a	—	—	-16	-15	—	—	—	—	—	—

P: P-Cygni profile; a: absorption; e: emission; *: different atmospheric and nebular velocities

Table 7. Radial velocity measurements (in km s⁻¹) associated to the Na I D (5889.95 and 5895.92 Å) and K I (7698.97 Å) lines detected in the post-AGB stars of our sample.

IRAS Name	K I 7699 Å		Na I 5890 Å		Na I 5896 Å	
	emission	absorption	emission	absorption	emission	absorption
01005+7910 *	n.d.	1, -6	20	-65, -41, -1	21	-65, -42, -1
02229+6208	n.d.	12, 29	n.d.	-2, 25	n.d.	-2, 24
04296+3429 *	-7	-18, 58	21	-17, 6, 56	21	-16, 6, 56
05113+1347 *	n.d.	-17, 2	-44	-17, 6	-43	-18, 5
05251-1244	n.d.	6	n.d.	4, -11	n.d.	5, -11
05341+0852	n.d.	14	23	21	23	21
06530-0213	—	—	n.d.	25, 47	n.d.	25, 46
07134+1005	n.d.	93	n.d.	29, 39, 91	n.d.	28, 40, 92
08005-2356 *	n.d.	24, -8, 48	-30	-47, 19	-30	-52, 17
08143-4406	n.d.	19, 4, 35	n.d.	16, 42, 61	n.d.	17, 42, 61
08544-4431	n.d.	27	n.d.	-42, 15, 39	n.d.	-41, 16, 43
12175-5338	n.d.	-5	31	-27, -6, 31	32	-27, -5, 32
16594-4656 *	n.d.	-10, -41, 5	14	-29, 6	13	-29, 8
17086-2403 *	n.d.	12	-6	17	-5	14
17097-3210	n.d.	5	n.d.	-29, 3	n.d.	-29, 3
17150-3224	10, 21, 2	n.d.	10	5	10	2
17245-3951	-1, 27	-86, -57	19	-98, -63, -31	19	-98, -66, -31
17395-0841	n.d.	17, 3	2	-1	3	-2
17423-1755	n.d.	11	3, 72	n.d.	3, 71	n.d.
17436+5003	n.d.	-50	n.d.	-66, -19	n.d.	-65, -19
18025-3906	n.d.	-89, -73	n.d.	-121, -34, 8	n.d.	-121, -31, 10
18062+2410	—	—	75	3, 20	67	3, 13
HD 172324	n.d.	6	n.d.	-28, 7	n.d.	-28, 8
19114+0002	n.d.	10, 67, 83	n.d.	11, 64, 127	n.d.	12, 65, 123
19200+3457	—	—	6	8	7	9
19386+0155	n.d.	10	—	—	—	—
19500-1709	n.d.	4, 22, -9	n.d.	2, 12, 20	n.d.	2, 14, 22
20000+3239	n.d.	2, 13	n.d.	-2, 21	n.d.	2, 21
20462+3416	n.d.	-21, -8	n.d.	-25, -6, 19	n.d.	-26, -7, 17
22023+5249	n.d.	-23	27, -130	-46, 2	27, -131	-46, 4
22223+4327	n.d.	-2, -30, -43	n.d.	-42, -18, 0	n.d.	-44, -18, 0
22272+5435	n.d.	-41	n.d.	-41, -4	n.d.	-41, -4
23304+6147 *	n.d.	-1, -12, -29	24	-52, -29, -7	24	-53, -29, -7

*: emission over absorption; —: spectral range not covered; n.d.: non detected

Table 8. Radial velocity measurements (in km s⁻¹) associated to the DBs detected in the post-AGB stars of our sample.

IRAS Name	Diffuse band								
	5780	5797	5850	6196	6284	6379	6614	6993	7224
01005+7910	-16	29*	—	-2	-9	2	-12	-16	—
02229+6208	32	-3*	—	33	52	22	—	24	—
04296+3429	66	—	—	—	55	59	60	—	—
05113+1347	8	—	—	—	—	—	0	—	—
05251-1244	-3	11	20	0	29	-14	0	—	—
05341+0852	—	—	—	—	—	4	—	15	37
06530-0213	—	—	—	—	26	33	12	—	—
07134+1005	-5	-14	2	—	—	—	5	—	—
08005-2356	—	30	36	—	—	—	—	—	—
08143-4406	—	—	6	—	20	12	24	16	16
08544-4431	23	—	16	-45*	19	17	28	5	8
12175-5338	11	2	-8	-7	-6	—	-4	—	—
16594-4656	—	—	9	6	9	6	2	-4	-3
17086-2403	14	—	—	—	—	—	2	—	—
17097-3210	—	—	3	5	5	-4	5	13	0
17150-3224	—	—	-1	—	-2	0	9	-3	1
17245-3951	—	—	—	—	27	-7	5	16	22
17395-0841	-10	17	—	8	0	3	3	—	-4
17423-1755	15	9	—	9	—	—	12	—	—
17436+5003	—	—	23	0	—	19	—	—	—
18025-3906	7	-35*	—	—	—	-36*	24	19	—
18062+2410	—	15	—	—	—	—	—	-1	—
HD 172324	39	-29*	—	—	—	—	—	—	—
19114+0002	34	—	6	19	12	8	—	-5	29
19200+3457	—	—	—	—	—	—	—	—	—
19386+0155	—	—	—	5	8	3	6	4	9
19500-1709	11	-44*	—	4	6	3	35*	—	9
20000+3239	15	—	—	6	35	1	—	—	12
20462+3416	-14	-4	45*	-14	5	-13	-9	—	-2
22023+5249	-21	-7	37*	-14	-17	2	2	0	-2
22223+4327	17	—	—	—	6	2	—	—	—
22272+5435	39	—	—	—	—	—	—	—	—
23304+6147	-3	—	—	-26	5	-8	—	—	—

* : likely contaminated measurement

List of Objects

‘NGC 6210’ on page 2	‘IRAS 19200+3457’ on page 3
‘NGC 7027’ on page 2	‘LS II +34 1’ on page 3
‘IC 351’ on page 2	‘IRAS 19386+0155’ on page 3
‘AFGL 2688’ on page 2	‘IRAS 19500-1709’ on page 3
‘IRAS 21282+5050’ on page 2	‘HD 187885’ on page 3
‘NGC 7027’ on page 2	‘IRAS 20000+3239’ on page 3
‘IRAS 21282+5050’ on page 2	‘IRAS 20462+3416’ on page 3
‘HR 4049’ on page 2	‘LS II +34 26’ on page 3
‘IRAS 07270-1921’ on page 2	‘IRAS 22023+5249’ on page 3
‘BD+30 3639’ on page 2	‘LS III +52 24’ on page 3
‘CPD-56 8032’ on page 2	‘IRAS 22223+4327’ on page 3
‘AC Her’ on page 2	‘BD+42 4388’ on page 3
‘WR137’ on page 2	‘IRAS 22272+5435’ on page 3
‘WR140’ on page 2	‘HD 235858’ on page 3
‘HR 4049’ on page 2	‘IRAS 23304+6147’ on page 3
‘HD213985’ on page 2	‘HD 172324’ on page 3
‘NCG 7027’ on page 2	‘HD 172324’ on page 4
‘HR 4049’ on page 2	‘HD 172324’ on page 4
‘IRAS 21282+5050’ on page 2	‘HD 172324’ on page 5
‘Red Rectangle’ on page 2	‘HD 183143’ on page 5
‘IRAS 04296+3429’ on page 2	‘HD 183143’ on page 6
‘HD 179821’ on page 2	‘IRAS 16594-4656’ on page 8
‘IRC+10216’ on page 2	‘IRAS 02229+6208’ on page 9
‘IRAS 01005+7910’ on page 3	‘IRAS 08544-4431’ on page 9
‘IRAS Z02229+6208’ on page 3	‘IRAS 02229+6208’ on page 10
‘IRAS 04296+3429’ on page 3	‘IRAS 08544-443’ on page 10
‘IRAS 05113+1347’ on page 3	‘IRAS 17086-403’ on page 10
‘IRAS 05251-1244’ on page 3	‘IRAS 17395-0841’ on page 10
‘IC 418’ on page 3	‘IRAS 17436+5003’ on page 11
‘IRAS 05341+0852’ on page 3	‘IRAS 18025-3906’ on page 11
‘IRAS 06530-0213’ on page 3	‘IRAS 18062+2410’ on page 11
‘IRAS 07134+1005’ on page 3	‘IRAS 16594-4656’ on page 11
‘HD 56126’ on page 3	‘IRAS 06530-0213’ on page 11
‘IRAS 08005-2356’ on page 3	‘IRAS 05341+0852’ on page 12
‘IRAS 08143-4406’ on page 3	‘IRAS 18025-3906’ on page 12
‘IRAS 08544-4431’ on page 3	‘IRAS 16594-4656’ on page 12
‘IRAS 12175-5338’ on page 3	‘HD 172324’ on page 13
‘SAO 239853’ on page 3	‘IRAS 16594-4656’ on page 13
‘IRAS 16594-4656’ on page 3	‘IRAS 05113+1347’ on page 13
‘IRAS 17086-2403’ on page 3	‘IRAS 18062+2410’ on page 13
‘IRAS 17097-3210’ on page 3	‘IRAS 18062+2410’ on page 13
‘HD 155448’ on page 3	‘IRAS 17086-2403’ on page 13
‘IRAS 17150-3224’ on page 3	‘IRAS 18062+2410’ on page 14
‘RAFGL 6815’ on page 3	‘IRAS 16594-4656’ on page 14
‘IRAS 17245-3951’ on page 3	‘IRAS 06530-0213’ on page 14
‘IRAS 17395-0841’ on page 3	‘IRAS 17245-3951’ on page 14
‘IRAS 17423-1755’ on page 3	‘IRAS 17086-2403’ on page 14
‘Hen 3-1475’ on page 3	‘IRAS 05341+0852’ on page 14
‘IRAS 17436+5003’ on page 3	‘IRAS 16594-4656’ on page 14
‘HD 161796’ on page 3	‘IRAS 17086-2403’ on page 14
‘IRAS 18025-3906’ on page 3	‘IRAS 17245-3951’ on page 16
‘IRAS 18062+2410’ on page 3	‘IRAS 19114+0002’ on page 16
‘HD 341617’ on page 3	‘IRAS 19114+0002’ on page 16
‘HD 172324’ on page 3	‘IRAS 17086-2403’ on page 16
‘IRAS 19114+0002’ on page 3	‘IRAS 17423-1755’ on page 16
‘HD 179821’ on page 3	‘IRAS 18025-3906’ on page 16
	‘IRAS 18062+2410’ on page 16